Tetramethylene[1]

Charles Doubleday, Jr.

Contribution from the Department of Chemistry, Columbia University, New York, New York 10027

Received May 6, 1993®

Abstract: Ab initio MCSCF and CI computations of the potential energy surface (PES) for the tetramethylene biradical lead to a new model for the stereochemical dynamics. The model postulates that tetramethylene loses stereochemistry during its formation and decay as well as during its lifetime. For example, *cis*-cyclobutane-1,2-d_2 can form tetramethylene with cisoid or transoid deuteration directly via the same transition state. This shared transition state model accommodates the different stereochemical properties reported experimentally in tetramethylenes generated from deuterated cyclobutane vs diazene precursors. The model describes a *generalized common biradical* in which the ratio of fragmentation to cyclization is independent of precursor but whose stereochemical properties may depend on the precursor. The computations detect shallow minima corresponding to gauche and trans biradicals that disappear when zero-point energy is included. Use of canonical variational transition state theory, with close attention to internal rotations, leads to the prediction that both gauche and trans conformers exist as entropy locked species at experimental temperatures. The gauche conformer is the common biradical intermediate deduced by experimentalists. On this PES the preference for allowed $2_s + 2_a$ cycloaddition is weakly maintained even though a biradical is involved. Of the seven saddle points located on the PES, at least four of them mediate more than one reaction. These reactions typically involve stereochemical changes, so that a given transition state leads to two stereochemically distinct products. This gives rise to the shared transition state model mentioned above and also to the conclusion that transition state theories cannot predict the stereochemistry of products derived from tetramethylene.

Introduction

A puzzling result stands out in the experimental literature on the 1,4-biradical, tetramethylene.[2-8] Thermolyses of deuterated cyclobutane[3] and diazene[2a] precursors, both presumed to proceed via tetramethylene as an intermediate, apparently lead to tetramethylenes with very different stereochemical properties. Interpreted in this way, the results seem inconsistent with the common biradical hypothesis,[2] according to which a reactive intermediate must have the same chemical properties no matter how it is formed. Since this hypothesis is a cornerstone of mechanistic analysis, it is important to investigate apparent violations of it, especially in an archetypal intermediate such as tetramethylene. This is a major goal of the paper, in which we present a description of the gas-phase dynamics of singlet-spin tetramethylene deduced from the ab initio potential energy surface (PES). Our calculations lead to a new model of tetramethylene as a *generalized common biradical* whose stereochemistry may depend on the precursor but whose fragmentation/cyclization product ratio is independent of precursor. We give an introductory summary of the model in the following paragraphs, prior to the full discussion later in the paper. This description is necessarily incomplete because we shall show that transition state theories cannot predict the stereochemistry of products derived from tetramethylene.

Previous *ab initio* computations of tetramethylene[9-13] have found shallow minima for the gauche and trans conformations which either disappear when corrected for the zero-point energy or survive only marginally.[12a] With Page, McIver, and King, we suggested some years ago that the gauche conformation lies in a free energy minimum protected from cyclization by an entropic barrier.[9] The barrier arises because cyclization is accompanied by a rapid decrease in entropy of internal rotation and other soft modes. The resulting increase in $-T\Delta S$ along the cyclization pathway can overtake the decrease in ΔH at a high enough temperature to produce an entropy-locked biradical. By the use of Truhlar's canonical variational theory[14] to calculate free energies of activation, the current calculations predict that gauche and trans conformers (Scheme I) exist at experimental temperatures as entropy-locked biradicals protected from cyclization and fragmentation by free energy barriers greater than RT.

Dervan and co-workers[2] presented a compelling argument for the existence of a tetramethylene derivative as a mechanistically significant intermediate based on the common biradical hypothesis mentioned above. A model used by experimentalists to describe the product stereochemistry[2-8] is shown in Scheme II, in which stereochemical scrambling is associated with the internal rotation process, k_{rot}. With D replaced by methyl in Scheme II, the

® Abstract published in *Advance ACS Abstracts*, November 15, 1993.

(1) (a) Dedicated to the memory of Gerhard L. Closs. (b) These results were presented in preliminary form on April 16, 1992 at the Joint US-Japan Seminar on New Aspects of Molecular Photochemistry in Photoconversion, Tsukuba, Japan, funded in part by the National Science Foundation.

(2) (a) Dervan, P.; Santilli, D. *J. Am. Chem. Soc.* **1980**, *102*, 3863. (b) Santilli, D.; Dervan, P. *J. Am. Chem. Soc.* **1979**, *101*, 3663. (c) Dervan, P.; Uyehara, T. *J. Am. Chem. Soc.* **1976**, *98*, 1262. (d) Dervan, P.; Uyehara, T.; Santilli, D. *J. Am. Chem. Soc.* **1979**, *101*, 2069. (e) Dervan, P.; Uyehara, T. *J. Am. Chem. Soc.* **1979**, *101*, 2076. (f) Schultz, P.; Dervan, P. *J. Am. Chem. Soc.* **1982**, *104*, 6660. (g) Dervan, P.; Dougherty, D. In *Diradicals*; Borden, W., Ed.; Academic Press: New York, 1982; p 107.

(3) Goldstein, M.; Cannarsa, M.; Kinoshita, T.; Koniz, R. *Stud. Org. Chem. (Amsterdam)* **1987**, *31*, 121.

(4) Lewis, D.; Glenar, D.; Kalra, B.; Baldwin, J.; Cianciosi, S. *J. Am. Chem. Soc.* **1987**, *109*, 7225.

(5) (a) Chickos, J.; Annamalai, A.; Keiderling, T. *J. Am. Chem. Soc.* **1986**, *108*, 4398. (b) Chickos, J. *J. Org. Chem.* **1979**, *44*, 780. (c) Wang, Y.; Chickos, J. *J. Org. Chem.* **1987**, *52*, 4776.

(6) Doering, W. *Proc. Natl. Acad. Sci. U.S.A.* **1981**, *78*, 5279.

(7) Gerberich, H.; Walters, W. *J. Am. Chem. Soc.* **1961**, *83*, 3935, 4884.

(8) Scacchi, G.; Richard, C.; Back, M. *Int. J. Chem. Kinet.* **1977**, *9*, 513, 525.

(9) Doubleday, C.; Camp, R. N.; King, H.; McIver, J., Jr.; Mullally, D.; Page, M. *J. Am. Chem. Soc.* **1984**, *106*, 447.

(10) Doubleday, C.; Page, M.; McIver, J. W., Jr. *J. Mol. Structure (Theochem)* **1988**, *163*, 331.

(11) Segal, G. *J. Am. Chem. Soc.* **1974**, *96*, 7892.

(12) (a) Bernardi, F.; Bottoni, A.; Celani, P.; Olivucci, M.; Robb, M.; Venturini, A. *Chem. Phys. Lett.* **1992**, *192*, 229. (b) Bernardi, F.; Bottoni, A.; Robb, M.; Schlegel, H. B.; Tonachini, G. *J. Am. Chem. Soc.* **1985**, *107*, 2260. (c) Bernardi, F.; Bottoni, A.; Tonachini, G.; Robb, M.; Schlegel, H. B. *Chem. Phys. Lett.* **1984**, *108*, 599.

(13) Borden, W. T.; Davidson, E. R. *J. Am. Chem. Soc.* **1980**, *102*, 5409.

(14) (a) Truhlar, D.; Icaacson, A.; Garrett, B. In *Theory of Chemical Reaction Dynamics*; Baer, M., Ed.; CRC Press: Boca Raton, 1985; Vol. IV, p 65. (b) Truhlar, D.; Garrett, B. *Annu. Rev. Phys. Chem.* **1984**, *36*, 159. (c) Truhlar, D.; Garrett, B. *Acc. Chem. Res.* **1980**, *13*, 440.

0002-7863/93/1515-11968$04.00/0

Scheme I

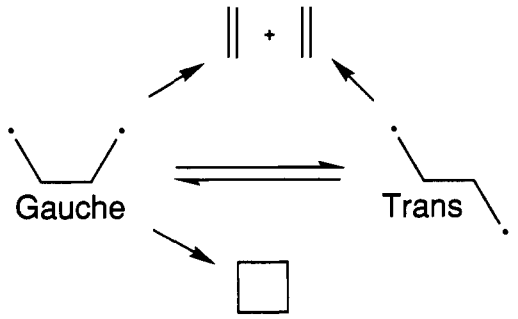

Scheme II

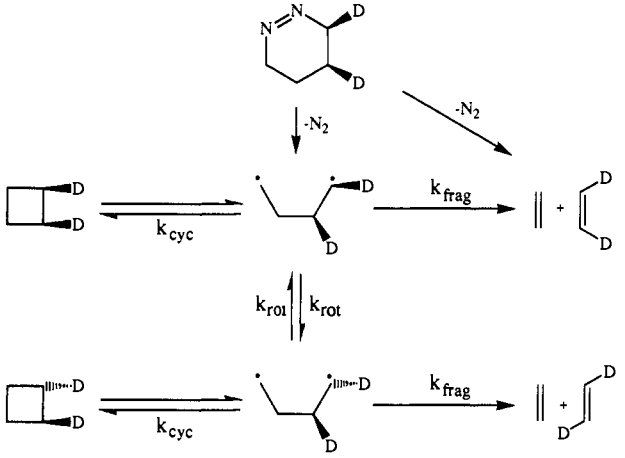

experimental ratio k_{rot}:k_{frag}:k_{cyc} was found to be the same starting from appropriate cyclobutane,[7] alkene,[8] or diazene precursors.[2c,e,g] The observation of identical ratios from different precursors implicates a single biradical common to all three modes of generation.

Similar evidence of a common biradical is incomplete for the deuterated parent tetramethylene of Scheme II. Dervan reported k_{rot}:k_{frag}:k_{cyc} = 12 ± 3:2.2 ± 0.2:1.0 at 712 K starting from the diazene,[2a,b,g] but no corresponding ratios have been reported for cyclobutane-*1,2-d*$_2$ or ethene precursors. Studies of cyclobutane-*1,2-d*$_2$[4,5] have yielded k_{frag}/k_{cyc} = 2.1 ± 0.1 at 693 K,[5a] but relative values of k_{rot} were not reported. However, Goldstein and coworkers[3] thermolyzed cyclobutane-*1,2,3,4-d*$_4$ (all cis) and reported k_{rot}:k_{frag}:k_{cyc} = 98 ± 2:1.2 ± 0.7:0.8 ± 0.5 at 693 K, or 120 ± 50:1.5 ± 1.1:1.0 with respect to k_{cyc} = 1. These ratios are very different from the diazene-derived ratios. Is it reasonable to suggest that a cyclobutane-derived tetramethylene is different from a diazene-derived tetramethylene?

Note that k_{frag}/k_{cyc} is the same within experimental error for the two precursors (2.2 ± 0.2 vs 1.5 ± 1.1) and is the same starting from cyclobutane-*1,2-d*$_2$,[4,5a] but k_{rot}/k_{cyc} = 12 ± 3 from the diazene and 120 ± 50 from cyclobutane. The biradical derived from cyclobutane-*d*$_4$ appears to be 10 times as stereorandom as that derived from the diazene. The difference is too large to be an isotope or temperature effect. It is not at all clear how to account for it using Scheme II or simple variations.[15]

Our calculations suggest a new model for biradical formation and decay, shown in Scheme III. We assume that tetramethylene is formed stereospecifically from the diazene, but we find that

Scheme III

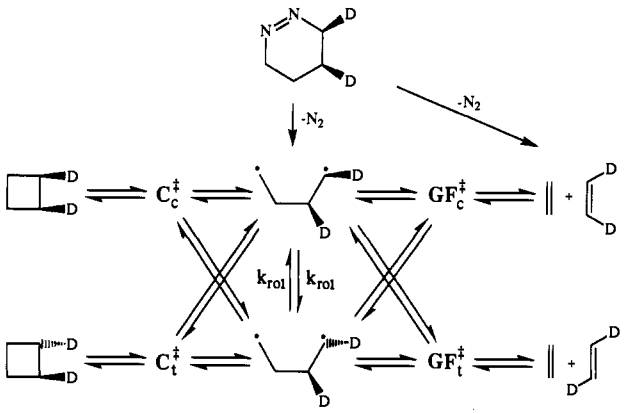

cyclobutane and 2 + 2 cycloaddition give tetramethylene stereorandomly via shared transition states **C**‡ (cyclization) and **GF**‡ (gauche fragmentation). For example, *cis*-cyclobutane-*1,2-d*$_2$ reaches the ring opening transition state C_c‡ (subscripts c and t indicate ciscoid and transoid deuteration) and then partitions between either of two biradical stereoisomers. A given biradical stereoisomer can form products via either of two isoenergetic diastereomeric transition states (negligible isotope effect). Each transition state does double duty, sharing reactions involving each biradical stereoisomer. (To make our assumptions clear, we display the shared transition states explicitly as if they were intermediates. Of course, the requirement of one-way passage through the transition states still holds!)

Scheme III is different in a fundamental way from the model of Scheme II or the twixtyl of Hoffmann et al.[16] Because Scheme III involves shared transition states, *stereorandomness is built into the formation and decay of the biradical*; k_{rot} is not necessary for stereochemical scrambling. In Scheme II the biradical is formed stereospecifically and scrambled via k_{rot}. Scrambling stops at the moment of product formation and the stereochemistry then present is transferred intact to the product. In the shared transition state model of Scheme III, scrambling occurs as the biradical is being formed and cannot be stopped by rapid product formation. In fact, product formation increases the scrambling because it constitutes an additional stereorandom step.

Cyclobutane thermolysis gives products via two independent stereorandom steps, formation and decay of the biradical, whereas diazene thermolysis involves only one stereorandom step, biradical decay. Therefore, Scheme III demands greater stereochemical scrambling in products derived from cyclobutane or 2 + 2 cycloaddition than from diazenes. This qualitatively resolves the stereochemical issue. It also requires that k_{frag}/k_{cyc} be independent of precursor because tetramethylene is involved in each case. The original notion of a common biradical having k_{rot}:k_{frag}:k_{cyc} independent of precursor is replaced by a *generalized common biradical* with k_{frag}/k_{cyc} invariant but whose stereochemistry depends on the precursor. These qualitative arguments will be made quantitative later in the paper.

The shared transition state model has an intrinsic uncertainty, namely that there is no way to predict the partitioning between stereoisomers obtained via the shared transition states **C**‡ and **GF**‡. Transition state theory cannot predict the product distribution in cases where two reactions share the same transition state; it is meant to predict only the *total* rate of unidirectional passage through the transition state. A full description of the stereochemistry of tetramethylene must await a more general dynamical treatment.

Scheme III is a major part of our story, but we have also found stereorandom *concerted* fragmentations and cycloadditions that share the same **C**‡ and **GF**‡ transition states. All of these

(15) A straw one might grasp is to assume the diazene extrudes N_2 one bond at a time to form an intermediate diazenyl biradical. One could postulate more restricted rotation in the diazenyl biradical than in tetramethylene (though theory[13] suggests the reverse, also see our results below) and require that at least some of the diazenyl biradicals yield products directly via intramolecular N_2 displacement without forming tetramethylene. These *ad hoc* assumptions might account for the relative stereochemistry, but would not explain why k_{frag}/k_{cyc} is independent of precursor.

(16) Hoffmann, R.; Swaminathan, S.; Odell, B.; Gleiter, R. *J. Am. Chem. Soc.* **1970**, *92*, 7091.

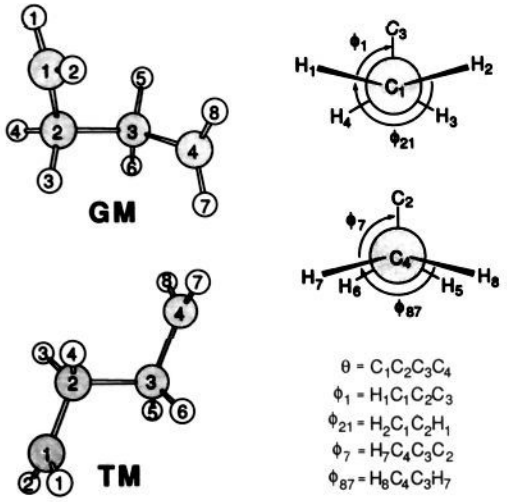

Figure 1. Atomic numbering system (left) and definition of torsion angles (right). The structures are those of the gauche and trans minima, **GM** and **TM** (see Table III). The torsion angle *abcd* is defined by viewing the four atoms along the *bc* vector with *b* in front and *c* in back: a clockwise rotation from *ab* to *cd* is defined as a positive angle, a counterclockwise rotation is negative. The pictures at right are for definition and illustration only and do not refer specifically to **GM** or **TM**.

results—the existence of tetramethylene as an intermediate, the discovery of shared transition states, and the possibility of stereorandom concerted fragmentation—are features that do not emerge from a standard quantum chemistry calculation in which one merely locates stationary points (minima and saddle points) on the PES. These features emerge only after exploring reaction paths leading down in energy from saddle points. We examined two types of paths. The intrinsic reaction coordinate (IRC), the steepest descent path in mass weighted Cartesian coordinates,[17] was used to calculate free energy barriers. Most of the stereochemical information came from non-IRC paths. Such a path starts at a saddle point and moves down in energy toward a product different from the product formed along the IRC path. These arbitrary paths have no dynamical significance other than that they reveal the energetic accessibility of processes not suggested by IRC paths.

Organizational Guide. There are three separate computations presented here, and Scheme III emerges only after considering all of them. First we discuss stationary points on the PES to get the basic energetics of tetramethylene and mention a connection with the Woodward–Hoffmann rules. Next we compute free energies along IRC reaction paths. This first requires a section on reaction path methodology with a description of how internal rotations are treated. The third type of computation involves non-IRC paths and leads directly to the model of Scheme III, which is discussed quantitatively at the end.

For those not interested in computational details, the basic information is contained in Table II and Figure 4 (energetics), Figures 6–8 (free energies), Table IV (product ratios), and Schemes III and V (stereochemistry), with the associated discussion in the text.

Geometrical Coordinates. The atomic numbering system is shown in Figure 1, applied to **GM** and **TM**, the gauche minimum and trans minimum on the PES. For discussing the internal rotations it is convenient to define the torsion angles θ, ϕ_1, ϕ_{21}, ϕ_7, and ϕ_{87}. θ is the torsion angle for internal rotation about the C_2C_3 bond. ϕ_1 and ϕ_7 describe internal rotation of H_1 and H_7 about the C_1C_2 and C_3C_4 bonds, respectively. ϕ_{21} and ϕ_{87} are torsion angles for H_2 and H_8, but they include H_1 and H_7 in their definitions and therefore indicate pyramidalization of the methylene groups. $\phi_{21} = 180°$ when the atoms H_1, C_1, C_2, and H_2 are in the same plane; deviation from 180° indicates pyramidalization of the radical center. $C_1H_1H_2$ torsion is therefore described by ϕ_1 and accompanying changes in pyramidalization by ϕ_{21}. For example, if ϕ_1 is roughly as shown in Figure 1, then $\phi_{21} > 180°$ implies that $C_1H_1H_2$ is pyramidalized toward C_3 and $\phi_{21} < 180°$ implies pyramidalization away from C_3. With ϕ_7 as shown, $\phi_{87} < 180°$ implies $C_4H_7H_8$ pyramidalization away from C_2.

Wave Functions and Basis Sets. Geometry searches and reaction paths were computed with a complete active space multiconfiguration self-consistent-field wave function[18a] with 4 electrons in 4 orbitals (4-in-4 CAS MCSCF, or 4-in-4) using the *MESA*[18b] programs. Complete CI within the active space of 4 electrons occupying 4 orbitals gives 20 configurations for the singlet spin state. The four active orbitals were the two singly occupied radical centers and the σ and σ^* orbitals of the C_2–C_3 bond. Stationary points were located with both 6-31G and 6-31G* basis sets,[19] and all were characterized by full analytical second derivatives. At geometries determined using 4-in-4/6-31G* the energies were recalculated using singles-and-doubles multireference CI (SDCI) using 6-31G*. This wave function includes single and double excitations from each configuration in the 4-in-4 CAS reference state. All such excitations were included except that the lowest four and highest four orbitals, mainly combinations of carbon 1s AOs, were required to remain doubly occupied and unoccupied, respectively. Of the 76 basis functions in the 6-31G* basis set 68 were involved in the CI: orbitals 1–4 were frozen core, 5–14 were doubly occupied in the reference, 15–18 were variably occupied in the reference (the CAS active space), 19–72 were virtuals, and 73–76 were frozen virtuals. This gives rise to 3 657 056 CSFs (configuration state functions) in C_1 symmetry, 1 829 134 CSFs in C_2 symmetry, and 921 182 CSFs in C_{2h} symmetry. The same SDCI/6-31G* wave function was also used to recalculate the energies of selected stationary points located on the 4-in-4/6-31G PES.

To test the frozen virtual approximation in the SDCI wave function, we compared the energies of the trans stationary points **TM** and **TF** (see geometries, next section) optimized with 4-in-4/6-31G* using SDCI/6-31G* energies calculated with and without frozen virtuals. Without frozen virtuals there are 72 orbitals involved in the CI and 1 062 082 CSFs in C_{2h} symmetry, and the energies of **TM** and **TF** are −156.500 006 and −156.499 595 hartrees, respectively. They differ by 411 μhartree, compared to a 512 μhartree difference with 4 frozen virtuals (Table II below). The difference of differences is 101 μhartree or 0.063 kcal/mol, and the use of frozen virtuals is justified.

Stationary Points on the PES. We found 10 stationary points for tetramethylene: 2 minima, 7 saddle points, and one second-order saddle point, located with 4-in-4 CAS and both 6-31G and 6-31G* basis sets. Analytical second derivatives were computed for each. Minima had all positive eigenvalues of the second derivative matrix, saddle points had one negative eigenvalue, and the second-order saddle point had two negative eigenvalues. The ten stationary points are described with their abbreviations in Table I. Table II lists the energies, zero-point vibrational energy (ZPE), and ZPE-corrected relative energies of the stationary points. Figure 1 shows the structures of **GM** and **TM**. Figures 2 and 3 show the structures of all other stationary points. Table III lists important structural parameters for the ten stationary points. The flat PES led us to stiffen the convergence criteria for geometry searches. One or more Newton–Raphson steps using analytical second derivatives generally brought the largest Cartesian gradient component, listed in Table III, to well under

(17) Fukui, K. *J. Chem. Phys.* **1970**, *74*, 4161.

(18) (a) Roos, B.; Taylor, P.; Siegbahn, P. *Chem. Phys.* **1980**, *48*, 157. (b) Molecular Electronic Structure Applications, written by Saxe, P.; Lengsfield, B., III; Martin, R.; Page, M.

(19) (a) Hehre, W.; Ditchfield, R.; Pople, J. A. *J. Chem. Phys.* **1972**, *56*, 2257. (b) Hariharan, P. C.; Pople, J. A. *Theor. Chim. Acta* **1973**, *28*, 212.

Table I. Glossary of Abbreviations for Stationary Points

stationary point	sym group	description of stationary point; *italicized mnemonics*
GM	C_2	*gauche minimum*
GF	C_2	saddle point for *gauche fragmentation*, starting from **GM**
GT	C_2	saddle point for *gauche-trans* interconversion (**GM-TM**)
G1	C_1	saddle point for *gauche* cyclization with *single* CH_2 twist
G2	C_2	saddle point for *gauche* cyclization with conrotatory *double* CH_2 twist
CT	C_1	saddle point for *cis-trans* isomerization of cyclobutane via single CH_2 twist
2N	C_2	stationary point for cyclization of **GM** with stereochemical retention; has *2 negative* eigenvalues of the second derivative matrix
TM	C_{2h}	*trans minimum*
TF	C_{2h}	saddle point for *trans fragmentation*, starting from **TM**
TR	C_s	saddle point for *trans rotation*; **TM** → **TM** with single CH_2 twist

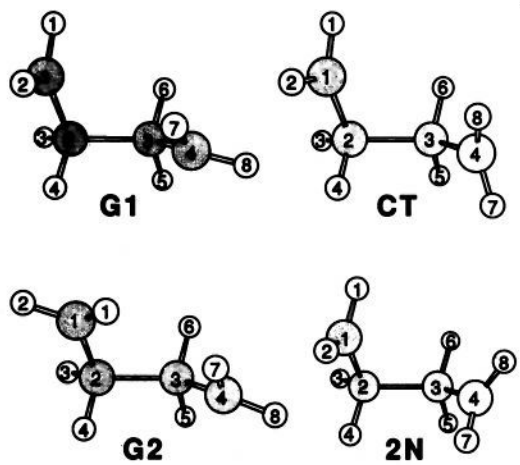

Figure 2. Molecular shapes of the stationary points involved in cyclization: **G1**, **G2**, **CT**, and **2N** optimized with 4-in-4/6-31G*. **G1** and **CT** have C_1 symmetry; **G2** and **2N** have C_2 symmetry. The atom numbers define the internal coordinates listed in Table III.

10^{-4} hartree/bohr. The supplementary material contains full geometries and frequencies obtained with both basis sets.

The barrier to fragmentation of cyclobutane was estimated by optimizing cyclobutane and **GM** with an 8-electron 8-orbital CAS wave function (1764 CSFs) and 6-31G* basis set and taking from Table II the 4-in-4/6-31G* energy difference between **GM** and **GF**. The 8-in-8 CAS active space consisted of the 4 σ and 4 σ^* C–C orbitals. Energies are –156.178 520 and –156.082 794 au for cyclobutane and **GM**, respectively. The ZPE of cyclobutane is 73.24 kcal/mol, from 8-in-8/6-31G* analytical second derivatives. The fragmentation barrier is 62.4 kcal/mol without ZPE and 57.2 kcal with ZPE correction. The experimental barrier is 62.5 kcal.[20] The energy of two ethenes separated by 1000 Å, calculated with 4-in-4 SDCI/6-31G* (921192 CSFs in C_{2v} symmetry), is –156.564 179 hartrees. Ethene optimized with 2-in-2/6-31G* has a ZPE of 33.48 kcal/mol. From the SDCI/6-31G* value for **GF** in Table II, the cycloaddition barrier is 45.7 kcal/mol without ZPE and 46.8 kcal with ZPE. Experiment gives an activation energy of 43.8 kcal.[21]

GM and **TM** are shallow minima on the 4-in-4/6-31G and 4-in-4/6-31G* PES. In both, the terminal CH_2 groups are pyramidalized slightly inward toward each other. **G1** is the saddle point connecting **GM** with cyclobutane via a single CH_2 twist. It is the lowest cyclization barrier. In Figure 2, as one looks at **G1** from C_4 to C_3, a clockwise (cw) twist of $C_4H_7H_8$ leads to **GM** (with H_7 and H_8 reversed relative to **GM** as defined in Figure 1) and counterclockwise (ccw) leads to cyclobutane. **G2** is the conrotatory double rotation saddle point for cyclization. A ccw twist of both methylene leads to cyclobutane and a double cw twist leads to **GM**. **CT** is the saddle point for concerted cis-trans isomerization of cyclobutane. Rotation of $C_4H_7H_8$ in either direction leads directly to cyclobutane, bypassing **GM**. **2N** is the barrier of cyclization of **GM** preserving C_2 symmetry. It has two negative eigenvalues of the second derivative matrix. One eigenvector is a conrotatory double rotation connecting **GM** with cyclobutane, preserving C_2 symmetry. The other is a disrotatory twist which breaks C_2 symmetry. Scheme IV shows interconversions among a representative set of stereochemically distinct structures involving gauche stationary points.

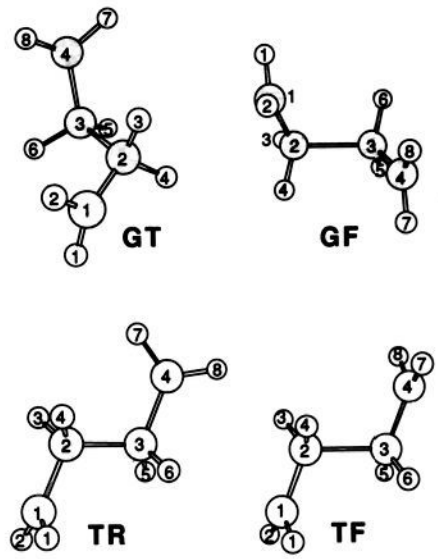

Figure 3. Molecular shapes of the stationary points **GT**, **GF**, and **TF** optimized with 4-in-4/6-31G* and **TR** optimized with 4-in-4/6-31G. **GT** and **GF** have C_2 symmetry, **TF** has C_{2h}, and **TR** has C_s. The atom numbers define the internal coordinates listed in Table III.

In Figure 3, **GT** is the saddle point connecting **GM** with **TM**. The transition vector[22] is θ rotation. **GF** and **TF** are the saddle points for fragmentation starting from **GM** and **TM**, respectively. Both transition vectors consist mainly of C_2C_3 stretching with smaller contributions from C_1C_2 and C_3C_4 contraction with rehybridization of the central two methylenes. **TR** is the saddle point for methylene rotation in **TM** and has C_s symmetry. It is the only stationary point located with 4-in-4/6-31G and not with 6-31G*.

Geometries are about the same with both basis sets. Bond lengths are generally the same to within 0.003 Å except for C_2C_3, which may differ by up to 0.03 Å. Bond angles show deviations of 0.2–0.8°. Even torsion angles show deviations of only ca. 1–3°. The exceptions are ϕ_{21} and ϕ_{87}, which describe pyramidalizations of the terminal methylenes. These angles are 4–9° greater with 6-31G* than with 6-31G.

Table II shows that the level of theory has little effect on relative energies. In fact, 4-in-4/6-31G gives very similar results to SDCI/6-31G* and is ≥100 times less expensive. Relative to **GM**, however, **GF** and **TF** are both higher on the 4-in-4/6-31G* PES than they are with either 4-in-4/6-31G or SDCI/6-31G*. Also, SDCI lowers the 4-in-4/6-31G* energies of **GF** and **TF**, which have similarly distorted geometries, by 1.5 kcal/mol relative to

(20) Value recommended by: Benson, S. *Thermochemical Kinetics*, 2nd ed.; Wiley-Interscience: New York, 1976. Based on data of: Douglas, J.; Rabinovitch, B.; Looney, F. *J. Chem. Phys.* **1955**, *23*, 315 (quoted in ref 4).

(21) Quick, L.; Knecht, D.; Back, M. *Int. J. Chem. Kinet.* **1972**, *4*, 61.

(22) The transition vector is the eigenvector associated with the imaginary frequency of the saddle point, originally defined in: McIver, J. W., Jr.; Stanton, R. E. *J. Am. Chem. Soc.* **1972**, *94*, 8618.

Table II. Potential Energy (in Hartrees), Relative Potential Energy, ZPE, and ZPE-Corrected Relative Energies (in kcal/mol) for All Stationary Points

	geometries optimized with 4-in-4/6-31G							geometries optimized with 4-in-4/6-31G*						
	4-in-4/6-31G				SDCI/6-31G*			4-in-4/6-31G*				SDCI/6-31G*		
	energy, au	E_{rel}[a]	ZPE[b]	E_{rel}[c]	energy, au	E_{rel}[a]	E_{rel}[c]	energy, au	E_{rel}[a]	ZPE[b]	E_{rel}[d]	energy, au	E_{rel}[a]	E_{rel}[d]
GM	−155.985 918	0.0	68.49	0.0	−156.492 814	0.0	0.0	−156.041 964	0.0	68.58	0.0	−156.492 758	0	0.0
GF	−155.984 484	0.90	68.14	0.56	−156.491 131	1.06	0.71	−156.038 245	2.33	68.04	1.79	−156.491 376	0.87	0.33
GT	−155.983 738	1.37	68.52	1.40	−156.490 835	1.24	1.27	−156.039 562	1.51	68.70	1.63	−156.490 719	1.28	1.40
G1	−155.985 131	0.49	68.06	0.08				−156.041 475	0.31	67.96	−0.31	−156.492 306	0.28	−0.34
G2	−155.983 555	1.48	68.12	1.11				−156.040 395	0.98	68.37	0.77	−156.490 230	1.59	1.38
CT	−155.983 886	1.28	68.07	0.86	−156.490 589	1.40	0.98	−156.040 459	0.94	67.90	0.26	−156.490 997	1.11	0.43
2N	−155.983 301	1.64	67.39	0.54				−156.039 488	1.55	67.27	0.24			
TM	−155.988 817	−1.82	68.82	−1.49				−156.045 292	−2.09	68.99	−1.68	−156.496 225	−2.18	−1.77
TF	−155.988 063	−1.35	68.39	−1.45				−156.042 554	−0.37	68.38	−0.57	−156.495 713	−1.85	−2.05
TR	−155.984 324	1.00	67.68	0.19										

[a] Energy relative to **GM** not including ZPE, in kcal/mol. [b] Zero-point vibrational energy, in kcal/mol, in the harmonic approximation. [c] Energy relative to **GM** including 4-in-4/6-31G ZPE, in kcal/mol. [d] Energy relative to **GM** including 4-in-4/6-31G* ZPE, in kcal/mol.

Table III. Important Bond Lengths (Å) and Torsion Angles (deg) for Stationary Points Optimized with 4-in-4/6-31G and 4-in-4/6-31G* and Largest Cartesian Gradient Component (10^{-5} hartree/Bohr)[a]

	G_{max}	C_1C_2	C_2C_3	C_3C_4	θ	ϕ_1	ϕ_{21}	ϕ_7	ϕ_{87}
GM 6-31G	2.2	1.4843	1.6266	1.4843	73.306	84.144	196.485	84.144	196.485
GM 6-31G*	5.5	1.4892	1.6044	1.4892	71.981	80.114	203.412	80.114	203.412
GF 6-31G	1.0	1.4470	1.7775	1.4470	81.437	80.541	196.068	80.541	196.068
GF 6-31G*	2.5	1.4381	1.8093	1.4381	84.849	77.100	200.896	77.100	200.896
GT 6-31G	3.8	1.4736	1.6775	1.4736	116.935	72.534	199.416	72.534	199.416
GT 6-31G*	3.2	1.4814	1.6432	1.4814	116.334	69.279	206.241	69.279	206.241
G2 6-31G	0.8	1.5004	1.5724	1.5004	66.584	−41.715	195.599	−41.715	195.599
G2 6-31G*	2.3	1.5007	1.5657	1.5007	65.624	−47.323	204.386	−47.323	204.386
2N 6-31G	0.5	1.5004	1.5798	1.5004	63.202	58.651	183.603	58.651	183.603
2N 6-31G*	17.9	1.5027	1.5679	1.5027	58.186	54.708	193.215	54.708	193.215
G1 6-31G	1.2	1.4961	1.5826	1.4958	66.567	63.756	183.956	−38.366	193.389
G1 6-31G*	2.7	1.4970	1.5715	1.4970	66.392	59.806	185.976	−38.382	202.219
CT 6-31G	0.2	1.5000	1.5799	1.4991	66.118	41.582	164.200	87.296	196.655
CT 6-31G*	0.4	1.4965	1.5823	1.4963	71.401	60.082	164.994	92.163	203.137
TM 6-31G	6.7	1.4780	1.6459	1.4780	180.000	79.389	201.222	79.389	201.222
TM 6-31G*	6.0	1.4833	1.6190	1.4833	180.000	75.989	208.021	75.989	208.021
TF 6-31G	3.8	1.4480	1.7705	1.4480	180.000	80.326	199.348	80.326	199.348
TF 6-31G*	15.1	1.4372	1.8073	1.4372	180.000	77.979	204.042	77.979	204.042
TR 6-31G	13.8	1.4989	1.5751	1.4991	180.000	82.534	194.916	0.000	180.000

[a] Full geometries are listed in the supplementary material.

Scheme IV

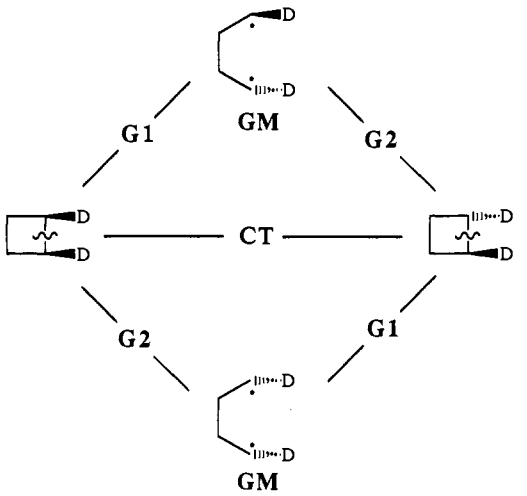

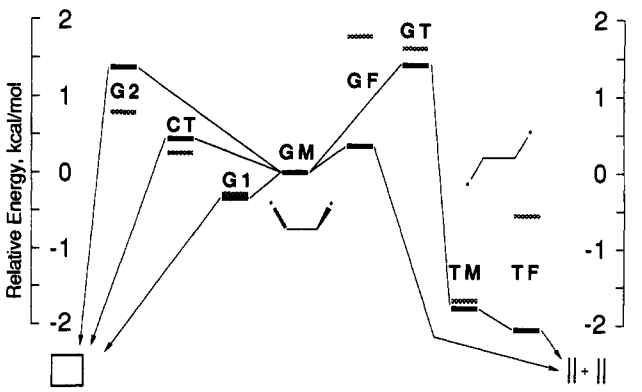

Figure 4. Relative potential energies including harmonic oscillator ZPE correction for eight stationary points optimized using 4-in-4/6-31G*, corresponding to the right half of Table II. Light shading: ZPE-corrected 4-in-4/6-31G* energies. Dark shading: ZPE-corrected SDCI/6-31G* energies. Lines connecting stationary points indicate some but not all of the energetically accessible pathways.

GM, a greater relative energy lowering than for any other stationary point.

G1, the lowest potential energy barrier protecting **GM**, disappears with ZPE-corrected 4-in-4/6-31G* (Table II). The trans biradical **TM** survives ZPE correction at the MCSCF level with both basis sets. At the most accurate level of theory, however—ZPE-corrected SDCI/6-31G* energies at geometries determined with 4-in-4/6-31G*—there is no local minimum corresponding to tetramethylene. At this level **G1** lies 0.34 kcal below **GM** and **TF** lies 0.28 kcal below **TM**. However, results below suggest that gauche and trans biradicals exist as *free energy* minima protected from decay by barriers $>RT$.

Figure 4 shows the relative ZPE-corrected energies of all stationary points except **2N** and **TR**. Lines connecting stationary points indicate the dynamical options. **GM** can fragment via **GF**, convert to the trans structure **TM** via **GT**, and cyclize with a single or double CH_2 twist via **G1** or **G2**. **CT** acts as an additional cyclization barrier, a role that will be discussed in a later section.

The trans biradical **TM** can fragment via **TF**, go back to gauche via **GT**, or undergo CH_2 internal rotation via **TR** (not shown).

Bernardi et al.[12a,23] have reported some of the stationary points in Table II, including **GM**, **GF**, **GT**, **TM**, and **TF**, located with 4-in-4 CAS and a double-ζ (DZ) basis set.[24] Relative energies and geometries were close to our 4-in-4/6-31G results. The main difference was that their use of ZPE-corrected multireference[25] second-order Møller–Plesset perturbation theory[26] (MP2) with the 6-31G* basis set did not erase the barrier to trans fragmentation, whereas SDCI/6-31G*+ZPE eliminates the barrier. The difference between SDCI and MP2 is not large: Table II gives barriers of 0.33 and −0.28 kcal/mol before and after ZPE correction, and the corresponding MP2 barriers are 1.36 and 0.75 kcal/mol.[12a] There may be an intrinsic difference between SDCI and MP2 in dealing with structures with distorted geometries such as **TF**. However, little can be inferred until the atomic basis set has been more fully explored.

Cyclization and the Woodward–Hoffman Rules. It surprised us that the lowest energy cyclization path involves a CH_2 twist (**G1**). At first we thought that **GM**, with C_2 symmetry, would cyclize via a saddle point with C_2 symmetry. The most obvious such structure is **2N**, which however has two negative eigenvalues of the second derivative matrix. Twisting is preferred because cyclization via **G1** is the final step of an allowed $2_s + 2_a$ cycloaddition, and cyclization via the higher energy **2N** is the final step of a forbidden $2_s + 2_s$ cycloaddition. The Woodward–Hoffmann[27] preference for $2_s + 2_a$ survives even in a biradical! This vestige of 4-center interaction is brought about by through-bond coupling controlled by CH_2 pyramidalization. The terminal CH_2 groups in **GM** are pyramidalized slightly *toward* each other, so that the orbitals point away from each other. As the biradical cyclizes, the nontwisting $C_1H_1H_2$, nearly planar at **G1**, pyramidalizes outward away from $C_4H_7H_8$ in order to bond with it.

Twenty years ago Dewar and co-workers,[28] using an analysis of through-bond coupling by Hoffmann et al.,[29] pointed out that inward and outward pyramidalizations in tetramethylene are favored by double occupancy of respectively the antisymmetric or symmetric orbital Ψ_A or Ψ_S as shown in Figure 5 for gauche structures. With outward pyramidalization (G_{out}) the two orbitals point toward each other, and this through-space overlap is favored by putting two electrons in Ψ_S.[30] With inward pyramidalization (G_{in}), through-space interaction is smaller than through-bond. Ψ_S is raised by mixing with the C_2–C_3 σ orbital and Ψ_A is lowered by mixing with σ^*. Therefore inward pyramidalization is favored by double occupancy of Ψ_A. G_{in} and G_{out} differ by the nodal

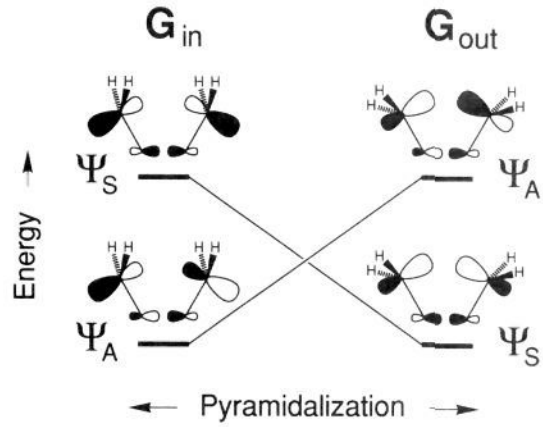

Figure 5. Orbital changes as a function of CH_2 pyramidalization in gauche structures G_{in} and G_{out}. Left: With inward pyramidalization of G_{in}, Ψ_A is pushed below Ψ_S as a result of interaction with σ^* of C_2C_3. Right: with outward pyramidalization of G_{out}, dominant through-space interaction places Ψ_S below Ψ_A. The lower energy orbital has a higher MCSCF occupation number, and the Ψ_S–Ψ_A crossing is associated with an energy barrier separating G_{in} from G_{out}. Orbital lobes of C_2C_3 are exaggerated in size for visibility. The maximum individual coefficients of C_2 and C_3 basis functions in Ψ_S and Ψ_A have magnitudes of ca. 0.05–0.12.

structures of their HOMO and LUMO. Dewar called such species lumomers, isomers whose interconversion involves a HOMO-LUMO crossing. Lumomeric interconversion encounters a barrier, a vestige of W–H *verbot*, which survives an MCSCF and even SDCI treatment. Since Ψ_S correlates with cyclobutane and Ψ_A correlates with two ethenes, the W–H rules for 2 + 2 cycloaddition *can be attenuated but not avoided by going through a biradical*.

The MCSCF results (here we use 4-in-4/6-31G*) bear out this picture. **GM** has a G_{in}-type structure with occupation numbers 1.16 and 0.84 for the appropriate natural orbitals which look like Ψ_A and Ψ_S, respectively. (**GF**, **GT**, **TM**, and **TF** also have inward pyramidalizations and are homomers[28b] of **GM**—their interconversion involves no HOMO-LUMO crossing and is W–H allowed.) An example of G_{out} is the cyclization transition state with arc length 5.0 on the path from **G1** to cyclobutane (see next section). This C_2 structure has occupation numbers 1.43 and 0.57 for Ψ_S and Ψ_A, respectively. The $2_s + 2_s$ cyclization[31] of **GM** that maintains C_2 symmetry passes through **2N**,[32] 1.24 kcal higher than the cyclization saddle point **G1**. The higher $2_s + 2_s$ barrier is associated with a Ψ_S–Ψ_A crossing as in Figure 5. Similar remarks apply to **CT**, in which the Ψ_S–Ψ_A crossing is traversed by consecutive instead of simultaneous outward paramidalizations (**CT** has one CH_2 pyramidalized inward and one outward). The $2_s + 2_a$ single twist via **G1** avoids the through-bond coupling that forces the Ψ_S–Ψ_A crossing.

One should keep in mind that the W–H stereochemical preference for single-twist cyclization exists in the potential energy; free energy is another matter. After describing free energy changes in tetramethylene, we shall return to the question of stereochemistry.

Reaction Paths and CVT: Method. To compute the free energies of activation for cyclization and fragmentation of the biradical we used the canonical variational theory (CVT) of

(23) Bernardi et al.[12a] reported two saddle points labeled TS1 and TS2 involved in cyclization of **GM**, optimized with 4-in-4/DZ and having maximum gradient components of 4.6×10^{-3} and 1.3×10^{-3} hartree/bohr, respectively. Only the geometry of TS1 was reported. In our notation it has torsion angles $\theta = 74.2°$, $\phi_1 = 113.4°$, $\phi_{21} = 169.6°$, $\phi_7 = 72.0°$, $\phi_{87} = 204.5°$ and a geometry intermediate between that of **CT** and **G1**. Using their 4-in-4/DZ wave function, we optimized **GM** and **CT** which we obtained with maximum gradient components of 4.0×10^{-5} and 3.7×10^{-7} hartree/bohr, respectively. Our **GM** geometry and energy agreed with theirs, and our **CT** geometry based on DZ was almost the same as our 6-31G result in Table III. These results plus their large gradients strongly suggest that TS1 and TS2 are not stationary and should be ignored.

(24) (a) Huzinaga, S. *J. Chem. Phys.* **1965**, *42*, 1293. (b) Dunning, T., Jr. *J. Chem. Phys.* **1970**, *53*, 2823.

(25) McDouall, J.; Peasley, K.; Robb, M. *Chem. Phys. Lett.* **1988**, *148*, 183.

(26) Møller, C.; Plesset, M. *Phys. Rev.* **1934**, *46*, 618.

(27) Woodward, R. B.; Hoffmann, R. *The Conservation of Orbital Symmetry*; Academic Press: New York, 1970.

(28) (a) Dewar, M. J. S.; Kirschner, S.; Kollmar, H.; Wade, L. *J. Am. Chem. Soc.* **1974**, *96*, 5242. (b) Dewar, M. J. S.; Kirschner, S. *J. Am. Chem. Soc.* **1974**, *96*, 5246. (c) Dewar, M. J. S.; Kirschner, S.; Kollmar, H. *J. Am. Chem. Soc.* **1974**, *96*, 5240.

(29) Hoffmann, R.; Imamura, A.; Hehre, W. *J. Am. Chem. Soc.* **1968**, *90*, 1499.

(30) We temporarily adopt the language of one-electron theory, in which the HOMO is doubly occupied and the LUMO is empty. In an MCSCF treatment the two approximately singly occupied natural orbitals, which resemble the Hartree–Fock HOMO and LUMO, have occupation numbers $1 + \delta$ and $1 - \delta$, where δ is usually ca. 0.1–0.2.

(31) It may seem improper to use the $2_s + 2_s$ or $2_s + 2_a$ designation, normally applied to the overall cycloaddition, to describe only half of the cycloaddition. In fact, these designations are indeed appropriate to the cyclization or ring opening step, because it is here that the orbital crossing can take place since **GM** and **GF** are homomeric with two ethenes. The 2 + 2 nature of biradical cyclization derives from through-bond coupling which allows all four centers to interact.

(32) **2N** is an interesting hybrid of G_{in} and G_{out}. The structure of **2N** resembles that of G_{in}, with less pyramidalization ($\phi_{21} = 193.2°$) than **GM** ($\phi_{21} = 203.4°$) as expected. However, the orbital ordering and occupation numbers (1.10 and 0.90 for Ψ_s and Ψ_A, respectively) resemble those of G_{out}.

Truhlar and co-workers.[14] In this method, the steepest descent path in mass-weighted Cartesian coordinates is calculated beginning at the saddle point and proceeding toward the reactant side and toward the product side of the PES. This path is known as the intrinsic reaction coordinate, or IRC,[17] and is generated by integrating $d\mathbf{x}/ds = -\mathbf{g}$, where $\mathbf{x}$ is the mass-weighted Cartesian coordinate vector,[33] $\mathbf{g}$ is the normalized gradient, and s is the arc length along the path in units of bohr·amu$^{1/2}$, defined so that $s = 0$ at the saddle point, $s < 0$ on the reactant side, and $s > 0$ on the product side. In practice the full IRC path from reactant to product does not have to be calculated and one only needs to examine the path within a few kilocalories per mole of the saddle point. Analytical second derivatives of the energy with respect to nuclear position are evaluated at intervals along the path. After projecting out the gradient direction and the overall rotations and translations, each mass-weighted second-derivative matrix is diagonalized to yield $3N - 7 = 29$ eigenvalues from which the partition function and thermodynamic functions are calculated. For a given temperature this procedure gives a set of free energies plotted against the arc length s along the path. The transition state is located at the top of this curve, which need not coincide with the saddle point on the PES. The rate constant k is calculated from the Eyring equation[34] with unit transmission coefficient, $k = (k_B T/h) \exp(-\Delta G^{\ddagger}/RT)$.

IRC paths were calculated with the Page–McIver algorithm[35] in the corrected local quadratic approximation.[36] In this method, analytical second derivatives at each point are combined with finite-difference third derivatives along the path direction to predict the next step. On a flat PES the path would become unstable if one or more of the $3N-7$ eigenvaluses of the projected second derivative matrix turned negative. In such a case the local reaction path valley flattens out and becomes a ridge. This did not occur in any of our paths. We used H masses to compute the paths, and the effect of deuteration was approximated by substituting D in the partition functions along the paths. This is not rigorous, because each deuteration pattern gives a different IRC path. However, we expect them not to stray far from each other in the region of the variational transition state, so we felt this would be a good approximation, and it allowed us to compute several deuteration patterns at once.

In addition to IRC paths, we also computed 8 non-IRC paths passing through **G1**, **CT**, **GF**, and **GT** and leading to products chemically distinct from the products described by the IRC paths (diastereomers or structurally different products). The non-IRC paths are shown as eight figures in the supplementary material. They were generated in internal coordinates (no mass weighting) with 4-in-4/6-31G by varying one or two torsion angles in small increments, typically 4–8°, accompanied at each step by ca. 1–4 constrained optimization cycles for all other coordinates. To justify the claim that the path energy stays below the saddle point energy, the eight supplementary figures show that the changes are small in *both energy and geometry* along the path. (If large increments are taken, the path can step over an energy ridge.) The reactions described by these paths will be discussed qualitatively in the section on stereochemistry.

To model the internal rotation entropy along the IRC paths, we replaced harmonic oscillator partition functions for internal rotation modes by appropriate internal rotation partition functions. In this paper computational tractability forced us to treat θ, ϕ_1 and ϕ_7 as independent. In fact, they are strongly coupled in certain regions of the PES though decoupled in other regions. In previous CVT calculations on radical and biradical reactions,[9,37] we fit rigid internal rotations to eq 1 and used approximate moments of intertia[38] to estimate

$$V(\phi) = \frac{V_0}{2}(1 - \cos(n\phi)) \tag{1}$$

partition functions. Use of approximate moments of inertia may lead to errors because of kinetic energy coupling of the 3 rotations and coupling to overall external rotation. Another possible problem is the single cosine term in eq 1. Along a reaction path the rotational potential often bears no resemblance to eq 1, and a more general Fourier series is needed.

These issues were avoided by solving the problem of kinetically coupled rotors, as follows. (1) The rotational potential energy curve was determined. We did this in two ways, by a rigid rotation keeping all other degrees of freedom fixed, and with relaxation of most other degrees of freedom (described below). Each curve had eight points, with angle ϕ = 0, 30, 60, 120, 180, 240, 300, 330°, with 0° defined to be the point on the reaction path. (2) For each ϕ the kinetic energy matrix[39] was computed, including all couplings among internal rotations and coupling between internal and external (overall) rotation. From the eigenvalues one calculates reduced moments of inertia, $I_r(\phi)$. (3) Energies were fit to eq 2 and $I_r(\phi)$ were fit to eq 3 with $B(\phi) = h/(8c\pi^2 I_r(\phi))$.[40]

$$V(\phi) = \frac{1}{2}\sum_{n=1}^{3}[V_n(1 - \cos(n\phi) + U_n \sin(n\phi)] \tag{2}$$

$$B(\phi) = B_0 + \sum_{n=1}^{3} B_n \cos(n\phi) + \sum_{m=1}^{3} B_m \sin(m\phi) \tag{3}$$

(4) Rotational wave functions were expanded in a basis of 50 sine and 50 cosine functions, matrix elements were computed[40] using the fitting parameters from step 3, and diagonalization gave the energy levels. Partition functions were calculated by explicit summation using all states. Use of 75 sine and 75 cosine terms did not change the partition functions.

Rotational energy curves were calculated with 4-in-4/6-31G. For rigid rotations we rotated θ and either ϕ_1 or ϕ_7, keeping all other internal coordinates fixed. Optimized rotations were computed similarly with optimization of all internal coordinates except θ, ϕ_1, and ϕ_7. Along fragmentation paths, C_2C_3 was also fixed to keep the molecule from moving along the path during rotation. Optimized rotations for **GM** and **TM** were deduced from stationary points already calculated. **GM**, **GT**, and **TM** are all on the same θ potential curve. Additional points were taken from the IRC path through **GT**. **CT** and **G1** both lie on the ϕ_1 curve for **GM**, and **CT** is the maximum (see below). C_{2h} symmetry of **TM** allowed us to use eq 1 for ϕ_1 rotation, with $n = 2$ and V_0 equal to the **TR-TM** energy difference.

We used optimized rotations instead of rigid rotations, based on comparisons in which rigid rotation overestimated the barrier height by 0.5–8.0 kcal/mol. Comparison of rotational curves calculated by 6-31G vs 6-31G* generally gave small differences. In the optimized θ rotation in **TF**, 6-31G and 6-31G* give almost superimposable curves with barriers of 8.9 and 9.2 kcal/mol, respectively. In the rigid θ and ϕ_1 rotations for **GM**, **CT**, **GF**, and **G1**, the difference in rotational barriers between the two basis sets is ca. 0.2–0.5 kcal.

Partition functions were computed for 1,2-dideuteriobutane-1,4-diyl. The free energies, ΔG, at each temperature were

(33) Mass-weighted Cartesian coordinates $\mathbf{x}(s)$ at arc length s along the path are defined by $\mathbf{x}(s) = \mathbf{M}^{1/2}\mathbf{q}(s)$ where $\mathbf{q}(s)$ is the Cartesian position vector (in bohr) of dimension $3N$ (N = number of atoms) and $\mathbf{M}$ is the $3N \times 3N$ diagonal matrix of triplets of atomic masses in amu.

(34) Glasstone, G.; Laidler, K.; Eyring, H. *Theory of Rate Processes*; McGraw-Hill: New York, 1941.

(35) Page, M.; McIver, J. W., Jr. *J. Chem. Phys.* **1988**, *88*, 922.

(36) Page, M.; Doubleday, C., Jr.; McIver, J. W., Jr. *J. Chem. Phys.* **1990**, *93*, 5634.

(37) (a) Doubleday, C.; McIver, J. W., Jr.; Page, M.; Zielinski, T. *J. Am. Chem. Soc.* **1985**, *107*, 5800. (b) Doubleday, C.; McIver, J. W., Jr.; Page, M. *J. Phys. Chem.* **1988**, *92*, 4367.

(38) Pitzer, K.; Gwinn, W. *J. Chem. Phys.* **1942**, *10*, 428.

(39) Kilpatric, J.; Pitzer, K. *J. Chem. Phys.* **1949**, *17*, 1064.

(40) Lewis, J.; Mallory, T., Jr.; Chao, T.; Laane, J. *J. Mol. Struct.* **1972**, *12*, 427.

constructed of three major parts: potential energy, harmonic free energy, and internal rotation free energy. We used SDCI/6-31G* potential energies at geometries optimized with 4-in-4/6-31G* for all stationary points except **TR**, for which 4-in-4/6-31G was used. Harmonic partition functions and thermodynamic functions[41] for the nonrotational modes were computed from analytical second derivatives using 4-in-4/6-31G* at stationary points and 4-in-4/6-31G along reaction paths. At a given temperature, each path was matched to its saddle point by applying to the path free energies the difference between the 6-31G* and 6-31G free energy at the saddle point. ΔG due to internal rotation was computed from optimized rotational barriers obtained with 4-in-4/6-31G. The harmonic ZPE and partition functions corresponding to internal rotations were identified from the eigenvectors of the force constant matrix projected onto internal coordinates and were replaced by internal rotation ZPE and partition functions. ΔG due to overall external rotation was computed with a classical partition function,[41] using moments of inertia that included the coupling with internal rotation.[39]

The IRC path for the cyclization of **GM** via **G1** was computed with a step size of 0.05 bohr·amu$^{1/2}$, and path energies were obtained as follows. At 9 points (s = 0.0, 1.0, 2.0, 3.0, 4.0, 5.0, 5.3, 5.6, 6.0 bohr·amu$^{1/2}$) the potential energy was recalculated using SDCI/6-31G*. The SDCI was based on a 2-in-2 CAS reference (633 966 CSFs in C_1 symmetry, 317 152 CSFs in C_2 symmetry) instead of 4-in-4. At these 9 points and also at s = 4.7[42] we calculated the partition functions and ZPE for optimized internal rotations[43] and substituted them for the corresponding harmonic values in the overall molecular partition function. To check that the 2-in-2 SDCI gave reasonable energy differences, we calculated the energy at s = 5.0 using SDCI/6-31G* based on the 4-in-4 CAS reference (1 829 134 CSFs in C_2 symmetry). The resulting 4-in-4 SDCI/6-31G* energy difference between the **G1** saddle point (s = 0) and the s = 5.0 point is 3.22 kcal/mol, compared to a difference of 3.42 kcal/mol using 2-in-2 SDCI/6-31G*. The 0.20-kcal discrepancy was incorporated into the path by assuming that the relative energies in the range s = 4.7–6.0 were well represented by 2-in-2 SDCI/6-31G*, but they were all corrected relative to the energy of **G1** (s = 0) by applying the 0.20-kcal correction uniformly between s = 4.7 and 6. In the range s = 0–4.7 the correction was assumed to vary linearly from 0 to 0.2 kcal.

A preliminary IRC path through **CT**, not shown in this paper, was calculated using 2-in-2/6-31G with a step size of 0.05 bohr·amu$^{1/2}$ and is discussed in the next section.

We had reported a path for fragmentation of **TM** via **TF**,[10] but we recalculated it here to have a uniform calculation of all paths. The IRC step size was 0.2 bohr·amu$^{1/2}$; 4-in-4/6-31G energies were recalculated with SDCI/6-31G* at s = 0, 0.2, 0.4, 0.6 in C_{2h} symmetry. SDCI energies at s = 0.8, 1.0 were estimated.[44] Partition functions were evaluated at s = 0, 0.2, 0.4, 0.6, 0.8, 1.0 using optimized rotations. For CH_2 rotation, C_{2h} symmetry allowed us to use eq 1 at each value of s, with n = 2 and V_0 determined by twisting one CH_2 by 90° and optimizing in C_s symmetry. For θ, an optimized rotation was computed at s = 0 (**TF**), which exhibited one maximum at θ = 0. For $s > 0$ only the optimized barrier maximum at θ = 0 was computed at each value of s, and each optimized θ curve was generated by assuming the shape of the curve was the same as for s = 0.

The IRC path for fragmentation of **GM** via **GF** was computed with a step size of 0.1 bohr·amu$^{1/2}$. Partition functions based on optimized internal rotations were calculated at s = 0, 0.1, 0.25, 0.4. SDCI calculations were done only for s = 0 (**GF**). SDCI corrections to the 4-in-4/6-31G path energies were taken to be the same as for the **TF** path.[45] The resulting error is probably small because **GF** and **TF** are similarly stabilized by SDCI (Table II, Figure 4), the 4-in-4/6-31G structures are similar, and the changes in C_2C_3 bond length and in other geometric parameters are similar along the two reaction paths.

CVT: Results and Discussion. We computed IRC paths passing through **G1**, **G2**, **CT**, **GF**, **GT**, and **TF**. IRC paths through **G2** and **GT** were calculated with a step size of 0.1 bohr·amu$^{1/2}$, in the range $-4.0 \le s \le 4.0$ for **GT** and $-1.6 \le s \le 3.0$ for **G2**.[46] The paths verify that **GT** interconverts **GM** with **TM** and that **G2** connects **GM** with cyclobutane. Preliminary application of CVT to these paths using harmonic partition functions showed that **G2** and **GT** are transition states at all temperatures we considered.

Figure 6 shows the changes in potential energy and free energy, ΔG, along the IRC path for cyclization of gauche tetramethylene-*1,2-d*$_2$ via **G1**. Deuterium atoms are shaded. The path begins at **GM** (s = −3.0) in C_2 symmetry (in the absence of deuteration), proceeds through **G1** (s = 0) in C_1 symmetry, and returns to C_2 symmetry at $s \approx 4$. Throughout the range $-3 < s < 6$ the path direction consists mainly of an internal rotation. For $-3 < s < 2$ the path direction is largely $C_4H_7H_8$ rotation, interrupted briefly at $-0.5 < s < 0.5$ to readjust the pyramidalization of $C_1H_1H_2$. In the range s = 4–6 the path direction consists mainly of θ rotation, plus a contribution from decreasing CCC angles.

ΔG at selected arc lengths s (circles and polygons) is plotted in Figure 6 relative to **GM** as the zero of energy at each temperature. The 0 K points are the SDCI/6-31G* relative potential energies corrected by 4-in-4/6-31G ZPE and matched to the SDCI/6-31G* energy of **G1** as described in the previous section. ΔG for **GF**, **CT**, **G2**, and **GT** are included for comparison. The 4-in-4/6-31G potential energy relative to **GM** is shown at each point on the path, as well as the potential energy corrected by the 4-in-4/6-31G harmonic ZPE. The sharp negative spikes in ZPE-corrected potential energy on either side of the saddle point and the broad dip at s = −0.8 are artifacts peculiar to this PES.[47] This does not affect the CVT estimate of the cyclization barrier.

The cyclization barrier is entropic. At 712 K the variational cyclization transition state **C**‡ (the same as in Scheme III) is located at s = 4.73 by quadratic interpolation and $\Delta G^{\ddagger}_{cyc}$ = 3.81 kcal/mol relative to **GM**, of which 0.97 kcal comes from ZPE.

(41) Herzberg, G. *Molecular Spectra and Molecular Structure*; Van Nostrand-Reinhold: New York, 1945; Vol. 2, Chapter 5.

(42) The required SDCI correction for s = 4.7 was interpolated from neighboring points.

(43) Optimized rotational potential energy curves were calculated only for the 7 points s = 0, 2.0, 4.0, 4.7, 5.0, 5.3, 5.6. Rigid-rotation curves were also calculated for s = 0, 1, 2, 3, 4, 5.6, 6.0. ΔG values for optimized internal rotation at s = 1, 3, 6 were estimated by applying the fractional change in ΔG for rigid rotations to the ΔG values for optimized rotations in the appropriate range of s. For example,

$$\Delta G^{s=1}_{\text{optimized}} = \Delta G^{s=1}_{\text{rigid}}\left(\frac{\Delta G^{s=2}_{\text{optimized}} - \Delta G^{s=0}_{\text{optimized}}}{\Delta G^{s=2}_{\text{rigid}} - \Delta G^{s=0}_{\text{rigid}}}\right)$$

(44) SDCI/6-31G* corrections to the 4-in-4/6-31G relative path energies at s = 0.2, 0.4, 0.6 were −0.13, −0.24, −0.28 kcal/mol, respectively (the SDCI path decreased more steeply than the MCSCF path). Extrapolation led to SDCI corrections of −0.32 and −0.36 kcal for s = 0.8 and 1.0, respectively. The uncertainty of these points probably does not matter because they lie below the fragmentation transition state.

(45) For the SDCI corrections to the 4-in-4/6-31G relative path energies, we used values of −0.06, −0.16, −0.24 kcal/mol at s = 0.1, 0.25, 0.4 bohr·amu$^{1/2}$, respectively.

(46) On the $s < 0$ side of the path, failure of the CPMCSCF linear equations to converge at s = −1.6 halted the computation. Unconstrained minimization starting from s = −1.6 led to **GM**.

(47) This is a result of not starting out exactly at the saddle point on a flat PES. Even with a tiny gradient (Table III) and the use of third derivatives along the transition vector, the first step from the saddle point strays from the path. The gradient at the resulting point, still very tiny, does not point exactly along the steepest descent direction as it should but contains some bond stretching components. When this gradient direction is projected out, the stretching components are removed from the ZPE which therefore plummets. As the gradient increases along the $s > 0$ path, the gradient vector approaches the steepest descent direction and the stretching components disappear from the path direction after a few steps. On the $s < 0$ side of the path the RMS gradient stays less than 2×10^{-5} hartree/bohr until s = −1.2 during which the path direction tends to lose its way on the flat PES. The **GF** and **TF** paths are much steeper and exhibit no such behavior.

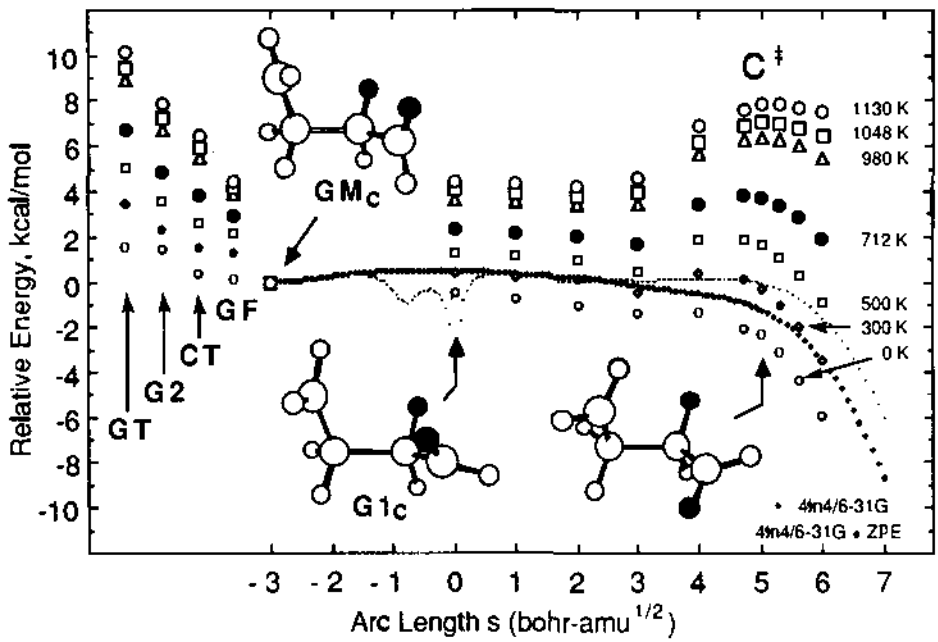

Figure 6. Energies relative to GM along the IRC path for cyclization of tetramethylene-1,2-d_2 via G1. The structures represent the starting material GM, the G1 saddle point, and s = 5.0 on the path. Subscripts "c" indicate cisoid deuterium (shaded atoms). 4-in-4/6-31G potential energies and ZPE-corrected energies are represented by a small "+" and dot, respectively. Circles and polygons represent free energies at the temperatures indicated at right, computed with SDCI/6-31G* potential energies and combined harmonic plus internal rotor partition functions as described in the text. At each temperature, the free energies of selected points along the path are plotted relative to the free energy of *GM* at that temperature. *C‡ is the* temperature-dependent variational cyclization transition state referred to in Scheme III, located at the top of the free energy curve. Free energies of four additional saddle points are shown at left.

(Exclusive use of harmonic partition functions for all modes gives $\Delta G^{\ddagger}_{cyc}$ = 1.31 kcal.) Eyring parameters are $\Delta H^{\ddagger}_{cyc}$ = -2.89 kcal and $\Delta S^{\ddagger}_{cyc}$ = -9.63 eu. The largest contribution to $\Delta S^{\ddagger}_{cyc}$ comes from θ rotation, which is the main component of the path direction at C‡. Loss of θ rotation on going from GM to C‡ contributes -7.13 eu to $\Delta S^{\ddagger}_{cyc}$. Restriction of the CH_2 rotations contributes -1.32 eu, and the remaining -1.18 eu comes from the $3N - 9$ = 27 nonrotational harmonic oscillator modes.[48] Figure 6 shows that as the temperature T rises, C‡ shifts to a more product-like geometry at a lower potential energy. This is also a shift toward lower entropy. These features compete to supress the T dependence of the cyclization rate constant, because $\Delta H^{\ddagger}_{cyc}$ is more negative but $-T\Delta S^{\ddagger}_{cyc}$ is more positive at higher T. This contributes to the small T dependence of the product ratios.

Note that $\Delta H^{\ddagger}_{cyc}$ = -2.89 kcal. In the range 693–1130 K the Arrhenius activation energy E_a is -1.4 kcal/mol (cyclization is slower at higher T). A negative E_a is usually discussed in terms of a two-step mechanism in which a reactive intermediate is lower in energy than the reactants.[49] The alternative entropic mechanism for negative E_a exemplified in Figure 6 is not confined to biradicals. At about the same time that we suggested entropic control of tetramethylene cyclization,[9] Houk and co-workers[50] presented a very similar but fuller discussion in an elegant study of carbene trapping. In our case and theirs, the negative E_a emerges from the requirement to locate the transition state by a ΔG criterion instead of a potential energy criterion. There is no paradox in locating the transition state at lower energy than the reactant. The mere existence of a molecule below the saddle point energy along the reaction path is not enough to guarantee product formation. In addition, its trajectory has to be headed in the right direction to form the product.

An important fact that led us to construct Scheme III is that C‡ is *effectively a branch point* for ring opening and cyclization paths, one branch connected via G1 to GM and the other to **CT**. The preliminary IRC path through **CT** mentioned briefly above (not shown in this paper) represents concerted cyclobutane isomerization; it connects *cis* and *trans*-cyclobutanes via a CH_2 twist without passing near GM. As cyclization begins, the **CT** path merges with the G1 path of Figure 6, as expected for two paths that both lead to cyclobutane. They are close at s = 4 on the G_9 path and indistinguishable at $s \geq 5.2$, $\theta = 50°$. In other words, the **CT** path connects **CT** with C‡, so that both concerted (via **CT**) and nonconcerted (G1) cyclization paths must pass through the C‡ region of the PES. Application of CVT along the **CT** path, after 2-in-2 SDCI/6-31G* correction of the energies, reveals at 712 K a nearly flat ΔG curve in the range $-6 < s < 5$ with no significant ΔG minimum. In Figure 6, ΔG of **CT** and C‡ (s = 4.73) are the same at 712 K. Above ca. 700 K, ΔG of C‡ rises above **CT** and C‡ *is the transition state common to both concerted and nonconcerted cyclizations*, which tends to blur the distinction between them. Below ca. 700 K the distinction is probably justified because ΔG of **CT** is greater than C‡.

Figures 7 and 8 show the IRC fragmentation paths passing through **GF** and **TF**, respectively. ΔG along each path at a given

(48) If most of the 3.8-kcal depth of the GM minimum comes from the loss of a single mode on going to C‡, it means that the inclusion of $3N - 6$ modes instead of $3N - 7$ is mainly responsible for placing GM in a free energy minimum. GM is legitimately included in the calculation because it is part of the path, but on a flat PES one worries about the discontinuity in the path energy at GM. It might be that a more realistic estimate of $\Delta G^{\ddagger}_{cyc}$ would be obtained by using not GM itself but a point on the reaction path slightly displaced from GM. Therefore we computed the partition function using 29 modes at s = 2.9 instead of 30 modes at s = -3.0, the actual GM minimum. At s = -2.9 the reaction path consists mainly of CHD rotation, whose removal decreases the entropy by 6.24 eu and the enthalpy by 1.39 kcal/mol at 712 K. This raises ΔG of GM by 3.1 kcal/mol, enough to put it above G1, which would become part of the new gauche ΔG minimum located between s = 0 and 3 in Figure 6 with a cyclization barrier of 2.1 kcal/mol at 712 K. The matter is not critical as long as the depth of the well is greater than RT. This discussion applies only to free energies of the shallow minima GM and TM, not to reaction paths or transition states. Therefore product ratios are unaffected.

(49) (a) Olson, L.; Koch, T. *J. Am. Chem. Soc.* **1986**, *108*, 756. (b) Maharaj, M.; Winnik, M. *J. Am. Chem. Soc.* **1981**, *103*, 2328. (c) Kisetev, V.; Millet, I. *J. Am. Chem. Soc.* **1975**, *97*, 4036.

(50) (a) Houk, K.; Rondan, N. *J. Am. Chem. Soc.* **1984**, *106*, 4293. (b) Houk, K.; Rondan, N.; Mareda, J. *Tetrahedron* **1985**, *41*, 1555.

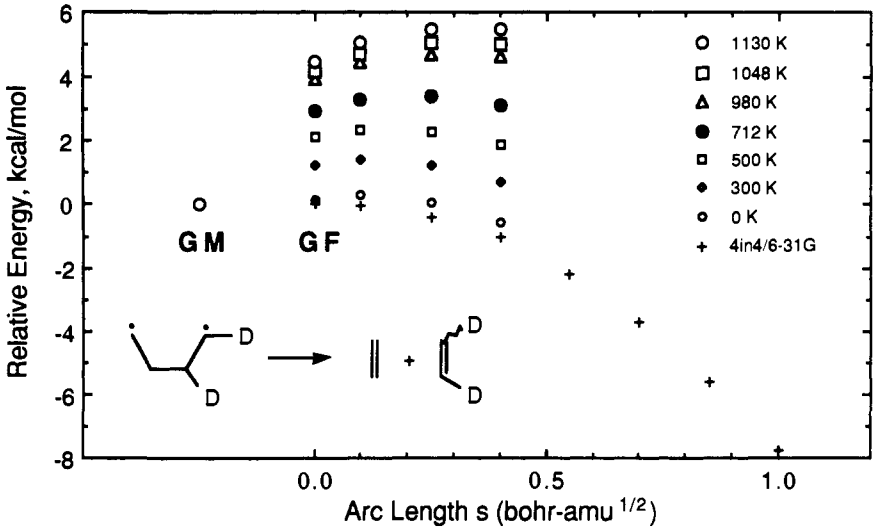

Figure 7. Energies relative to GM along the IRC path for fragmentation of gauche tetramethylene-*1,2-d*$_2$ via GF. 4-in-4/6-31G potential energies are represented by a "+". Circles and polygons represent free energies at the temperatures listed at right, plotted relative to GM exactly as in Figure 6. Free energies were computed only at s = 0.0, 0.1, 0.25, 0.4. Formally part of the path, GM is shown for comparison at left in an unlabeled section of the abcissa.

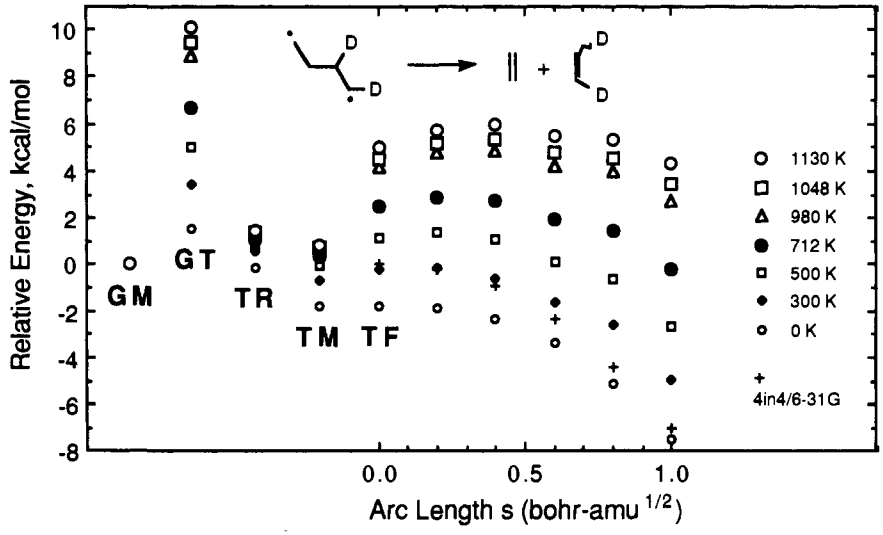

Figure 8. Energies relative to GM along the IRC path for fragmentation of *trans*-tetramethylene-*1,2-d*$_2$ via TF. 4-in-4/6-31G potential energies are represented by a "+". Circles and polygons represent free energies at the temperatures listed at right, plotted relative to GM exactly as in Figure 6. Relative free energies of TM, formally part of the path, are shown for comparison at left in an unlabeled section of the abcissa, along with the relative free energies of TR, GT, and GM, the zero of energy. TR free energies are based on 4-in-4/6-31G and harmonic partition functions as described in the text.

temperature is plotted relative to GM at that temperature. In Figure 8, ΔG of GT, TM, and TR[51] are included for comparison.

TM is entropy locked.[52] With TR below the fragmentation transition state at high enough temperature, stereochemical scrambling is important in *trans*-tetramethylene, even though at 0 K the barrier for CH_2 rotation via TR is 1.68 kcal/mol[53] and the fragmentation barrier is nil. At 712 K, $\Delta G^{\ddagger}_{rot}$ = 0.70 kcal/mol and $\Delta G^{\ddagger}_{frag}$ = 2.57 kcal/mol at s = 0.24 bohr·amu$^{1/2}$ by quadratic interpolation, giving TM a rotation to fragmentation ratio (k_{rot}/k_{frag}) of 3.7. At 1130 K $\Delta G^{\ddagger}_{rot}$ = 0.63 kcal and $\Delta G^{\ddagger}_{frag}$ = 5.12 kcal (s = 0.36), giving k_{rot}/k_{frag} = 7.4. Cyclization, available only via GT, is much slower than fragmentation. At 712 K, the rate of passage over Gt is only 7% of the fragmentation rate and 16% at 1130 K. These are upper bounds to the actual percentage of cyclization. According to results described below, a significant but unknown fraction of trans biradicals does not cyclize but passes from TM to GT to GF to two ethenes. Evidently the main role of TM is to allow cis-trans isomerization of ethene-d_2 by forming TM, twisting via TR, and cleavage. Largely isolated from cyclization, TM appears not to be the experimentalists' common biradical intermediate.[2-6]

For trans fragmentation at 712 K, $\Delta H^{\ddagger}_{frag}$ = −1.4 kcal, $\Delta S^{\ddagger}_{frag}$ = −5.5 eu, $\Delta G^{\ddagger}_{frag}$ = 2.6 kcal, and $\Delta ZPE^{\ddagger}$ = 0.2 kcal. CH_2 rotations contribute −3.2 eu to $\Delta S^{\ddagger}_{frag}$ and θ rotation contributes −0.24 eu, the remainder coming from nonrotational harmonic modes. Though this is a fragmentation, $\Delta S^{\ddagger}_{frag} < 0$ because CH_2 rotation is restricted in the transition state as the double bonds form. The mode directly responsible for fragmentation, C_2C_3, is the reaction coordinate and does not contribute to $\Delta S^{\ddagger}_{frag}$. At

(51) TR was optimized only with 4-in-4/6-31G; no SDCI correction was made and no internal rotation partition functions were calculated. The free energy of TR was computed relative to TM, based on 4-in-4/6-31G energies and harmonic oscillator partition functions for both.

(52) Recalculating ΔG of TM as we did for GM in ref 48 by using $3N-7$ modes instead of $3N-6$ had hardly any effect. At 712 K, use of $3N-7$ modes by removing the lowest vibration of A_g symmetry (the symmetry of the reaction path), 380 cm^{-1}, raises the ΔG of TM-*1,2-d*$_2$ by only 0.3 kcal/mol in contrast to 3.1 kcal for GM. In TM the ZPE is lowered by 0.54 kcal, while loss of the partition function (=1.87) raises the free energy by only 0.88 kcal. By contrast, in cyclization of GM the mode lost at s = −2.9 is a CHD rotation with ZPE = 0.16 kcal and a partition function of 11.0.

(53) The existence of a large CH_2 rotation barrier in TM had been noted in ref 13.

Table IV. Free Energies of Activation (kcal/mol) and Relative Rates for Fragmentation and Cyclization of Gauche Tetramethylene-*1,2-d*$_2$ with Separate Parameters Included for Fragmentation via **GF** and **GT**

T (K)	$\Delta G^{\ddagger}_{cyc}$	$\Delta G^{\ddagger}_{frag,GF}$	$\Delta G^{\ddagger}_{frag,GT}$	$k_{frag,GF}/k_{cyc}$	$k_{frag,GT}/k_{cyc}$	k_{frag}/k_{cyc}	k_{frag}/k_{cyc}, expt
500	2.00	2.41	5.02	0.66	0.05	0.71	
600	2.84	2.89	5.81	0.96	0.08	1.04	
693	3.67	3.31	6.56	1.30	0.12	1.42	2.1 ± 0.1,[a] 1.5 ± 1.1[b]
712	3.83	3.39	6.71	1.36	0.13	1.49	2.2 ± 0.2[c]
800	4.68	3.83	7.42	1.71	0.18	1.89	
900	5.65	4.33	8.23	2.09	0.24	2.33	
980	6.43	4.72	8.88	2.41	0.28	2.69	
1048	7.11	5.07	9.44	2.66	0.33	2.99	1.3 ± 0.5[d]
1130	7.95	5.48	10.12	3.00	0.38	3.38	2.7 ± 0.6[d]
1200	8.64	5.85	10.7	3.22	0.42	3.64	

[a] Reference 5a, from the value of $\Delta\Delta G^{\ddagger}$ reported in ref 4. [b] Reference 3, for tetramethylene-*1,2,3,4-d*$_4$. [c] Reference 2a. [d] Reference 4, from the reported values of $\Delta\Delta G^{\ddagger}$.

712 K, exclusive use of harmonic partition functions gives $\Delta G^{\ddagger}_{frag}$ = 0.40 kcal instead of 2.6. Harmonic frequencies do not reflect the actual tightening of the CH_2 torsions at the transition state.

Fragmentation/Cyclization Product Ratios. Using the steady-state kinetic assumption for **GM** and **TM** in Scheme I we can calculate k_{frag}/k_{cyc}, the ratio of total fragmentation to cyclization in tetramethylene. The calculation is simplified by results below, which show that any gauche or trans biradical passing through **GT** can fragment directly without going through **TM** or **GM**. This effectively turns **GT** into an additional transition state for fragmentation of **GM** or **TM**. If we ignore **TM** and concentrate on **GM** as the only significant tetramethylene intermediate, we get $k_{frag}/k_{cyc} = [\exp(-\Delta G^{\ddagger}_{frag,GF}/RT) + \exp(-\Delta G^{\ddagger}_{frag,GT}/RT)]/\exp(-\Delta G^{\ddagger}_{cyc}/RT)$, where $\Delta G^{\ddagger}_{cyc}$, $\Delta G^{\ddagger}_{frag,GF}$, and $\Delta G^{\ddagger}_{frag,GT}$ are free energies of activation for passage from **GM** to respectively the ΔG maxima along the **G1** path (i.e., **C**‡), along the **GF** path, and over the **GT** saddle point.

Table IV lists the values of $\Delta G^{\ddagger}_{cyc}$, $\Delta G^{\ddagger}_{frag,GF}$, and $\Delta G^{\ddagger}_{frag,GT}$ at various temperatures and the calculated and experimental k_{frag}/k_{cyc} ratios. The agreement with experiment is reasonable. The temperature dependence of k_{frag}/k_{cyc} is predicted and observed to be weak over the range 693–1130 K. The theoretical ratio increases faster than the observed ratio. The largest deviation from experiment is at low temperature, although the experimental values do vary. On balance, CVT accounts for the main features of the experimental k_{frag}/k_{cyc} ratios between 693 and 1130 K.

The biradical lifetime is virtually independent of temperature in this range. From 693 to 1130 K, the Arrhenius activation energies calculated from Table IV are E_{cyc} = −1.4 kcal, $E_{frag,GF}$ = +1.6 kcal, and $E_{frag,GT}$ = +2.7 kcal. The activation energies for cyclization and **GF** fragmentation nearly cancel, and the biradical lifetime $\tau = (k_{cyc} + k_{frag,GF} + k_{frag,GT})^{-1}$ is calculated to be τ = 0.40 ps at 693 K and τ = 0.33 ps at 1130 K.

Non-IRC Paths and Stereochemistry. Tetramethylene loses stereochemistry because the PES is flat. It turns out that the flatness also allows stereochemically distinct reactions to share the same transition state as shown in Scheme III. That is, in addition to the IRC path leading from a saddle point to a given stereoisomer, a non-IRC path also proceeds from the same saddle point down to a product different from the IRC product (a diastereomer or structurally different product). A non-IRC path is not a steepest descent path and has no unique definition. Its only significance is that it reveals an energetically accessible avenue to a non-IRC product, which by construction has the same energetic accessibility as the IRC product. If energetic accessibility implies dynamical accessibility,[54] then transition state theories cannot predict the product ratio, other than a ratio of 1.

Examples are known in which the IRC bifurcates below the saddle point and leads to two local minima instead of one.[55,56] Marcus has analyzed several of these as part of a general discussion of topographical criteria for the inapplicability of transition state theory.[57] Tetramethylene is different. We encountered no IRC branch points, but searched for and found non-IRC paths leading to *chemically distinct* products, as opposed to enantiomeric products[55] or the same products with different symmetries.[56]

The results described in this section lead to the shared transition state model of Scheme III. To show this we need to describe the ways in which the transition states are shared. In Figures 1–8 of the supplmentary material we report energies and geometries of eight non-IRC paths passing through **G1**, **CT**, **GF**, and **GT**, computed as described above in the section on reaction path methods. Below we give a qualitative summary of the results. Each of Figures 9–13 bears on a different aspect of Scheme III. Non-IRC paths through **G1** (Figure 9) bear on k_{rot} in Scheme III; paths through **CT** (Figures 10, 11) are related to **C**‡ since an IRC path connects **C**‡ with **CT**; paths through **GF** (Figure 12) are related to **GF**‡; paths through **GT** (Figure 13) are related to the discussion of Table IV and our conclusion that **GM** is the significant conformer of tetramethylene.

We found that a set of **G1** structures interconverts via a *coupled disrotatory motion* of both CH_2 groups. This is a gear motion with C–H bonds as the cogs (Figure 9). The rotation barrier is ≈0 (actually 0.065 kcal/mol). With the deuteration pattern of Figure 9, the coupled gear rotation accounts for optical isomerization of cyclobutanes. *trans*-Cyclobutane opens via **C**‡ to a set of interconverting **G1** and **GM** structures all with cisoid deuteration,[58] labeled $\mathbf{G1}_c$ and $\mathbf{GM}_c$. Similar opening of *cis*-cyclobutane would give a set of interconverting $\mathbf{G1}_t$ and $\mathbf{GM}_t$ biradicals exactly as in Figure 9. The sets of cisoid and transoid **G1** and **GM** structures can interconvert via **CT** in a process described below.

Double gear rotation accounts for cis-trans isomerization of cyclobutane-*1,2-d*$_2$ if one of the CH_2–CHD bonds cleaves to form tetramethylene-*1,2-d*$_2$. In this case the coupled gear motion would mimic single rotation because only one terminal methylene is labeled. In contrast to Figure 9, this deuteration pattern would allow the gear rotation to interconvert cisoid and transoid **G1** and **GM** structures. Thus the paths of lowest potential energy for both geometric and optical isomerization of cyclobutane-*1,2-d*$_2$ involve the coupled gear rotation of **G1** structures. We can use this to compute k_{rot}/k_{cyc} in Scheme III. At 712 K, ΔG of **G1** is 1.5 kcal lower than **C**‡, which gives $k_{rot}/k_{cyc} = \exp(-1.5/RT)$ = 2.9.

(54) In the absence of classical trajectories, an energetically accessible process must be taken seriously as a candidate for dynamical accessibility because it meets one of the requirements.

(55) (a) Valtazanos, P.; Ruedenberg, K. *Theor. Chim. Acta* **1986**, *69*, 281. (b) Kraus, W.; DePristo, A. *Theor. Chim. Acta* **1986**, *69*, 309.

(56) (a) Baker, J.; Gill, P. *J. Comput. Chem.* **1988**, *9*, 465. (b) Bosch, E.; Moreno, M.; Lluch, J.; Bertran, J. *Chem. Phys. Lett.* **1989**, *160*, 543.

(57) Marcus, R. A. *J. Phys. Chem.* **1991**, *95*, 8236.

(58) Cisoid ($\mathbf{GM}_c$, $\mathbf{G1}_c$) and transoid biradicals ($\mathbf{GM}_t$, $\mathbf{G1}_t$) are defined as follows. If one rigidly rotates θ so that θ = 0 (4 carbons coplanar) with all other degrees of freedom fixed, the biradical is cisoid if the two deuteriums are on the same side of the carbon plane and transoid if they are on opposite sides.

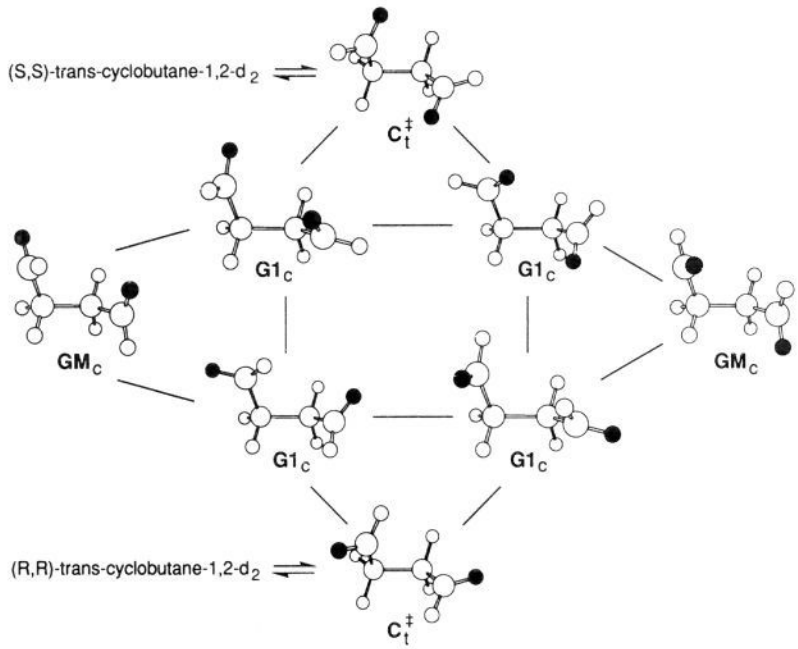

Figure 9. Ring opening of *trans*-cyclobutane to a family of interconverting $\mathbf{G1}_c$ and $\mathbf{GM}_c$ biradicals with exclusive cisoid deuteration, indicated by shaded atoms (see ref 58). Since **G1** structures are saddle points rather than minima, arrows are replaced by lines to indicate energetic accessibility between connected structures.

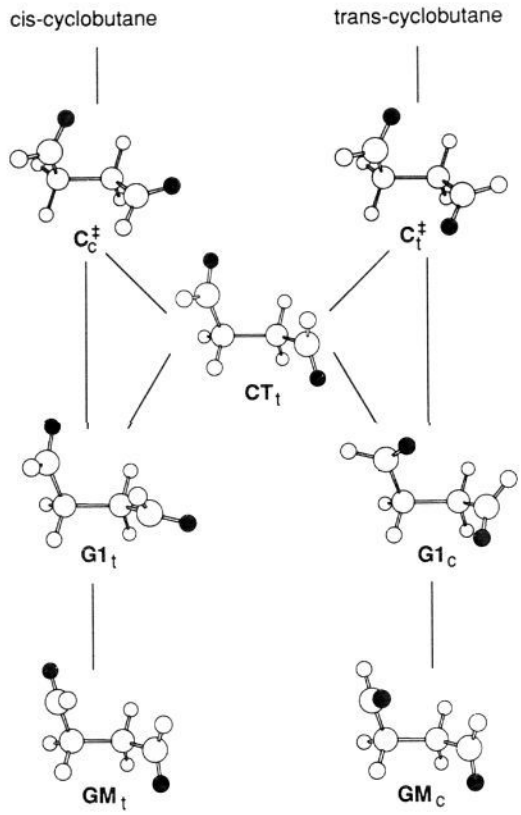

Figure 10. Energetically accessible paths connecting cyclobutane-*1,2-d*$_2$ with gauche tetramethylene-*1,4-d*$_2$ via **CT**, showing that cis and trans biradicals **GM** are accessible from the same ring-opening transition state **C‡** (the variational cyclization transition state of Figure 6). Shaded atoms are deuterium. Subscripts c and t indicate cisoid and transoid deuteration, defined in ref 58. Lines connecting structures indicate bidirectional energetic accessibility.

The **CT** saddle point, in addition to mediating the IRC path for concerted cis-trans isomerization of cyclobutane, also mediates cis-trans isomerization of **GM** as shown in Figure 10. The non-IRC portion of the path is $\mathbf{G1}_t$–$\mathbf{CT}_t$–$\mathbf{G1}_c$; all others are IRC paths. Passage between **GM** and **CT** does not actually require the molecule to go through **G1** as shown, because the non-IRC path is arbitrary and a variety of similar paths accomplish the same thing. (For example, we found an additional $\mathbf{CT}_t$–$\mathbf{GM}_t$ path that misses $\mathbf{G1}_t$, the right-hand CH_2 twisting much less than in $\mathbf{G1}_t$.) Figure 10 was chosen to exhibit the choices that are energetically accessible to a path from one saddle point to another.

In Figure 10, *cis*-cyclobutane can open with retention of stereochemistry via $\mathbf{C}_c^{\ddagger} \rightarrow \mathbf{CT}_t \rightarrow \mathbf{G1}_c \rightarrow \mathbf{GM}_c$ and with inversion via $\mathbf{C}_c^{\ddagger} \rightarrow \mathbf{G1}_t \rightarrow \mathbf{GM}_t$.[59] In ring opening and cyclization, *retention and inversion have equal energetic accessibility* via the same **C‡** transition state. Keeping in mind that entropy favors **CT** over **C‡** and that at 712 K **CT** and **C‡** have the same ΔG, one sees that **GM** is ΔG accessible from cyclobutane via **C‡** → **CT** followed by 0 twist ($2_s + 2_s$, *trans*-cyclobutane → $\mathbf{GM}_t$) or two twists ($2_a + 2_a$, *cis*-cyclobutane → $\mathbf{GM}_c$) or else with a $2_s + 2_a$ single twist via **G1**.[31] At **C‡**, **CT**, and **G1**, trajectories are presented with a choice that involves both a question of stereochemistry and a question of concert. None of the decisions is predictable by transition state theories.

Figure 11 shows the stereochemistry of tetramethylene-*1,2-d*$_2$ resulting from **CT**-mediated ring opening. The possibilities are greater than in Figure 10 because the CH_2 or CHD group in **C‡** can rotate either clockwise (cw) or counterclockwise (ccw). Discussion is simplified by considering unidirectional conversion of *trans*- to *cis*-cyclobutane. **C‡** is converted to **GM** via **G1** by a CH_2 or CHD twist. In the **CT**-mediated processes, cw and ccw CHD twists yield either **GM** with two different stereochemistries or *cis*-cyclobutane concertedly. **CT**-mediated CH_2 twisting is ignored.

Above ca. 700 K the free energy of **CT** drops below **C‡**. With **C‡** as the transition state common to all cyclizations and ring

(59) In discussing the energetic feasibility of the non-IRC paths in this section we use free energy as the primary criterion and potential energy elsewhere. For example, we assume that **CT** is energetically accessible from **C‡** on the basis of its free energy, even though **CT** is higher than **C‡** in potential energy. The claim of energetic feasibility for the non-IRC path from **CT** to **G1** to **GM** is based on the fact that (1) **G1** and **GM** are lower than **CT** in both free energy and potential energy and (2) the potential energy of the path itself never rises above **CT**. Since a non-IRC path has no uniquely defined free energy, we use its potential energy plus the free energy of the end points in judging energetic feasibility.

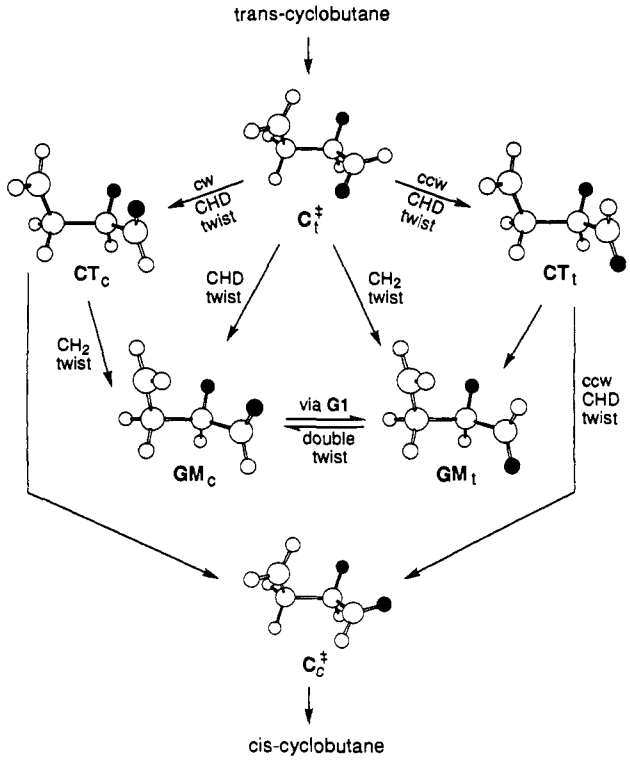

Figure 11. *trans*-Cyclobutane → *cis*-cyclobutane isomerization via tetramethylene-*1,2-d*$_2$ structures. The same paths are used as in Figure 10, but the stereochemical possibilities are larger. For simplicity **G1** is not shown. **C**‡, the transition state for ring opening, can undergo either a CH_2 twist or a CHD twist, either clockwise (cw) or counterclockwise (ccw). Formation of **GM** from **C**‡ or **CT** occurs via **G1** as in Figure 10.

openings, Figures 9–11 show that *cyclobutane can form, and be formed from, diastereomeric biradicals via the same C‡ transition state.* The possibility of otherwise concerted trajectories branching off at **CT** and becoming nonconcerted suggests that the concerted and nonconcerted mechanisms may merge. Above 712 K with **CT** below **C**‡, it may be justified to speak of a single nonconcerted mechanism.

The sharing of a single transition state **C**‡ among several rotations bears more than a passing resemblance to Doering's "continuous diradical as transition state",[60] originally proposed for substituted cyclopropane isomerizations. In Doering's description, three distinct internal rotations (two single twists and a double twist) compete in the same region of the trimethylene PES, and somewhere in this region are located the transition states for all 3 reactions. If the 3 reactions do actually share the same transition state then transition state theory cannot predict the product ratios. This is actually the situation that emerges for the parent trimethylene, discussed briefly in the final section.

The **GF** saddle point mediates 3 processes. The IRC path connects **GM** with two ethenes with retention of stereochemistry. We found 2 non-IRC paths. One is a nonconcerted path **GF** → **G1** → **GM** with disrotatory twisting of both CH_2 groups. The other is a concerted pathway that converts **GF** directly to cyclobutane with a single CH_2 twist ($2_s + 2_a$ cycloaddition), bypassing **GM**. The overall effect is that *a single GF transition state mediates formation and fragmentation of both diastereomeric biradicals.*

The situation is shown in Figure 12, where the deuteration pattern allows the double twist to mimic a single twist. The concerted $2_s + 2_a$ single twist may yield either retained or inverted stereochemistry, via CH_2 or CHD rotation. Of the nonconcerted paths, the IRC 0 twist and non-IRC double twist paths give biradicals with retained and inverted stereochemistry, respectively, which can lose stereochemistry via the gear rotation of **G1**.

(60) Doering, W. von E.; Sachdev, K. *J. Am. Chem. Soc.* **1974**, *96*, 1168.

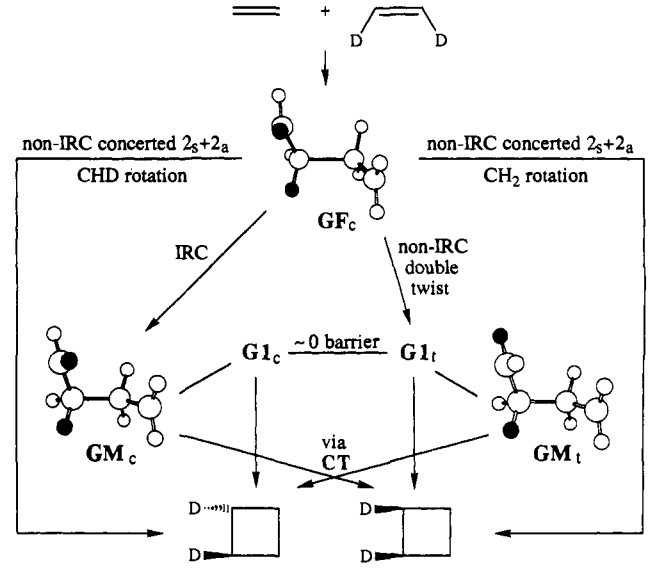

Figure 12. IRC and non-IRC reactions that proceed via the **GF** saddle point, exemplified by cycloaddition of ethene + *cis*-ethene-*d*$_2$. The IRC connects **GF** to **GM** with no methylene twist. A nonconcerted non-IRC path connects **GF** to **GM** with a double disrotatory twist, and a concerted non-IRC path connects **GF** directly with cyclobutane with a single methylene twist. **GM** cyclizes with either stereochemistry by processes described in Figures 10 and 11.

The concerted $2_s + 2_a$ cycloaddition in Figure 12 is another W–H example. We searched for a concerted path without methylene twisting, $2_s + 2_s$, requiring the path energy to stay below **GF**. However, a $2_s + 2_s$ path must climb the lumomeric ridge[28] separating **GF**, with methylenes paramidalized inward, from the cyclobutane side of the ridge having outward pyramidalization. Without climbing the lumomeric ridge, the $2_s + 2_s$ path moves toward **GM**, a homomer[28b] of **GF** with similar pyramidalization. Likewise the $2_a + 2_a$ double twist path leads to **GM** rather than cyclobutane. The $2_s + 2_a$ path leads from **GF** to cyclobutane and *not* to **GM**, as we found when we performed an extensive but unsuccessful search to find a single twist path from **GF** to **GM** without rising higher in energy than **GF**. On the tiny energy scale of this flat PES, the W–H rules are gently but consistently enforced: *concerted or not, cyclization prefers* $2_s + 2_a$. Nonconcerted cycloaddition takes **GF** to **GM** with either 0 twist (IRC) or 2 twists (non-IRC) and subsequent cyclization with 1 twist via **G1** lead to *net* $2_s + 2_a$ stereochemistry. All processes share the same saddle point **GF** as well as the same variational cyclization transition state **C**‡.

The IRC path through **GT** connects **GM** and **TM** via θ rotation. We found 4 non-IRC paths, in which **GT** mediates concerted cyclization and fragmentation with either retention or inversion of stereochemistry. **GT** is evidently higher than the local lumomeric ridge and the paths experience no W–H stereochemical preference.

Figure 13 shows the reactions mediated by GT_t (transoid deuteration). The IRC path connects GM_t with TM_t. The concerted cyclization paths start at **GT** and proceed directly to cyclobutane bypassing **GM** and **G1**, to give retained stereochemistry or single epimerization. Concerted fragmentation paths proceed toward ethylene as θ is moving in either the gauche or trans direction, bypassing either **GM** or **TM**. Since cyclization and fragmentation each occur independently with 0 or 1 twist, the overall cycloaddition or cycloreversion via **GT** can occur with 0, 1, or 2 twists. If one considers only the fragmentation paths, **GT** is just a brief encounter of two ethenes which collide, rotate about the C_2C_3 bond, and separate with optional CH_2 twisting. Thus **GT** mediates concerted cis-trans isomerization of ethene-*d*$_2$ *without intervention of a biradical intermediate.* The relatively low entropy of **GT** (as a result of losing θ rotation at the transition

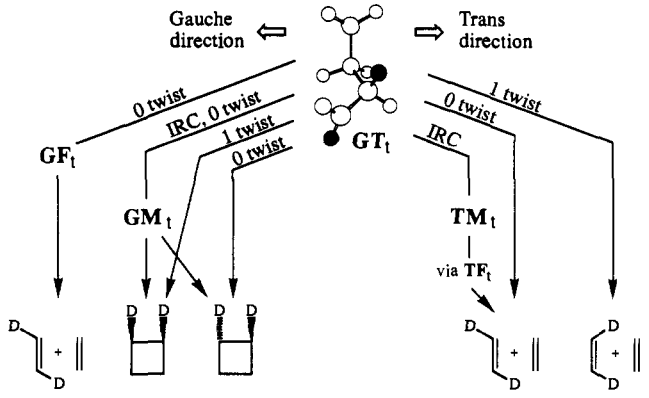

Figure 13. Summary of chemical reactions mediated by GT, exemplified by transoid deuteration (subscript t, shaded atoms) on carbons 1 and 2. The processes are classified according to the direction of movement (gauche or trans) along the θ-twist transition vector. The number of methylene twists involved in each process is also shown. The IRC path is labeled; all others are non-IRC. For simplicity, the single twist paths refer only to CHD twisting; CH_2 twisting is ignored.

Scheme V

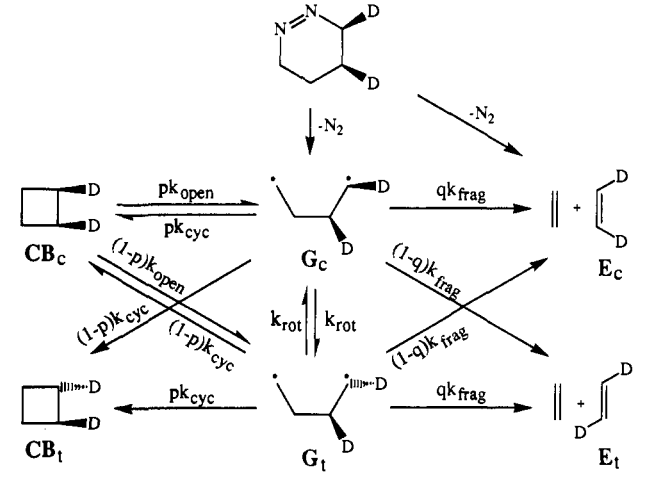

state) gives it a free energy 2.9 kcal higher than **C**‡ at 712 K, making **GT**-mediated processes slower by a factor of 7.8. At 1130 K this changes to 2.2 kcal and a factor of 2.7.

Shared Transition State Model. We have enough information now to justify the model of Scheme III. Figures 9–11, plus the fact that ΔG of **C**‡ is above **CT** at >700 K (Figure 6), imply that ring opening of cyclobutane-*1,2-d*$_2$ gives rise to either stereoisomeric biradical via the same transition state **C**‡, and that a single **C**‡ mediates cyclization from either stereoisomer. Figure 12 shows that fragmentation or cycloaddition via both stereoisomeric biradicals can be mediated by the same transition state **GF**‡. A variety of concerted reactions are also possible (via **CT** and as shown in Figures 12 and 13), but for reasons already discussed the biradical mechanism is likely to dominate.

For a quantitative treatment we use Scheme V, a version of Scheme III suitable for kinetic analysis. For simplicity, the only precursors considered are *cis*-diazene and *cis*-cyclobutane-*1,2-d*$_2$. p and q are partitioning fractions for retention, and Scheme V imposes the simplifying approximation that diastereomeric transition states partition identically. Because of the shared transition states, a pair of arrows from a given point of origin are not independent and must be considered together. When $p = q = 1$, Scheme V reverts to Scheme II. When $p = q = 0.5$ biradical formation and decay are completely stereorandom. If the actual system conforms to Scheme V with, say, $p = q = 0.6$, analysis of experimental results according to Scheme II would yield a large *apparent* k_{rot}/k_{cyc} ratio even if $k_{rot} = 0$ for rotation in the biradical.

The effect of the number of stereorandom steps on net retention in the products is easy to compute. Setting $p = q = 0.6$ and $k_{rot} = 0$ gives a surviving stereoisomeric excess of $p - (1 - p) = 2p - 1 = 0.2$ in favor of retention for one sterorandom step (e.g., reaction of *cis*-cyclobutane, **CB**$_c$, to form 60% **G**$_c$ and 40% **G**$_t$). Fragmentation of **CB**$_c$ requires two stereorandom steps and gives ethene products with respective fractions of retention and inversion equal to $p^2 + (1 - p)^2$ for 2 retention or 2 inversion steps and $2p(1 - p)$ for inversion–retention or retention–inversion. Net retention in the ethenes is equal to $p^2 + (1 - p)^2 - 2p(1 - p) = (2p - 1)^2 = 0.04$ even if $k_{rot} = 0$. If k_{rot} is significant the scrambling is greater.

With **CB**$_c$ or *cis*-diazene as starting material, steady state kinetic analysis of Scheme V yields the relation between the kinetic parameters (k_{rot}/k_{cyc} and k_{rot}/k_{frag}) and experimental product ratios, e.g., the fraction of net retention in biradical-derived products and the fragmentation/cyclization ratio. Defining the net retention in biradical-derived cyclobutanes as $([CB_c] - [CB_t])/([CB_c] + [CB_t])$ and similarly for ethenes **E**$_c$ and **E**$_t$, we get

$$\frac{[CB_c] - [CB_t]}{[CB_c] + [CB_t]} = \frac{(2p-1)([G_c] - [G_t])}{[G_c] + [G_t]} = \frac{(2p-1)^n}{1 + 2(k_{rot}/k_{cyc})_{calc}F_{cyc}} \quad (4)$$

$$\frac{[E_c] - [E_t]}{[E_c] + [E_t]} = \frac{(2q-1)([G_c] - [G_t])}{[G_c] + [G_t]} = \frac{(2p-1)^m(2q-1)}{1 + 2(k_{rot}/k_{frag})_{calc}F_{frag}} \quad (5)$$

$$F_{cyc} = \frac{k_{cyc}}{k_{cyc} + k_{frag}} \qquad F_{frag} = \frac{k_{frag}}{k_{cyc} + k_{frag}}$$

where $n = 1, 2$ (eq 4) and $m = 0, 1$ (eq 5) according to the number of stereorandom steps in the mechanism, and the subscript "calc" refers to the ratio computed by CVT. At 712 K $(k_{rot}/k_{cyc})_{calc} = 2.9$ and $(k_{rot}/k_{frag})_{calc} = 1.9$. If $p = q$, p is the only adjustable parameter in eqs 4 and 5 since F_{cyc} and F_{frag} are determined from product ratios. The same experimentally determined net retention, analyzed in terms in Scheme II with **CB**$_c$ or *cis*-diazene as starting material, gives the following result,

$$\frac{[CB_c] - [CB_t]}{[CB_c] + [CB_t]} = \frac{[E_c] - [E_t]}{[E_c] + [E_t]} = \frac{[G_c] - [G_t]}{[G_c] + [G_t]} = \frac{1}{1 + 2\dfrac{k_{rot}}{k_{cyc} + k_{frag}}} = \frac{1}{1 + 2R_aF_{cyc}} \quad (6)$$

$$R_a = (k_{rot}/k_{cyc})_{apparent}$$

in which F_{cyc} is the same as above and the subscript "apparent" refers to the apparent k_{rot}/k_{cyc} ratio obtained by analyzing experimental results in terms of Scheme II, thereby assigning all stereochemical scrambling to the rotation step k_{rot} in the biradical. In Scheme II the net retention must be the same in cyclization and fragmentation products, but in Scheme V the two products may have different amounts of retention if $p \neq q$. With **CB**$_c$ or *cis*-diazene as starting material and $p = q$, k_{cyc}/k_{frag} is given by the ratio of trans products $[CB_t]/[E_t]$. This means that F_{cyc} or F_{frag} values determined by analyzing experiments according to Scheme II can be used directly in eq 4 or 5 if one assumes $p = q$.

As discussed in the introduction, the k_{rot}:k_{frag}:k_{cyc} ratios reported by Goldstein[3] from *all-cis*-cyclobutane-*1,2,3,4-d*$_4$ at 693 K were 120 ± 50:1.5 ± 1.1:1.0, and those reported by Dervan[2a] from the *cis*-diazene in Scheme V at 712 K were 12 ± 3:2.2 ± 0.2:1.0. In terms of eq 6, $R_a = 12 \pm 3$ from the diazene precursor and 120

± 50 from cyclobutane-d_4. Below we show that a single choice of p in Scheme V basically reproduces both experimental R_a values. The fit is close to exact if one makes a kinematic assumption involving no additional parameters—that CH_2 rotation is favored over CHD rotation in tetramethylene-*1,2*-d_2 because of its smaller mass. Both stereoisomeric biradicals can be formed via the same C* transition state. If they are equally likely the biradical is stereorandom, $p = 0.5$. On average, however, CH_2 rotation (retention) may be faster than CHD rotation (inversion) if CH_2 and CHD twisting have equal amounts of kinetic energy. For a given value of the rotational kinetic energy, $I_r\omega^2/2$, the ratio of angular velocities (ω) is related to the reduced moments of inertia (I_r) as $\omega(CH_2)/\omega(CHD) = (I_r(CHD)/I_r(CH_2))^{1/2} = 1.21$, with I_r computed from the full rotational kinetic energy matrix.[39] If one considers the reorientation of a classical free rotor,[61] the autocorrelation function is Gaussian in time with a width proportional to $I_r^{1/2}$, which leads again to the factor of 1.21. If this factor is fully realized as a stereochemical preference it corresponds to $p = 0.55$, which adds $2p - 1 = 0.1$ to the single-step net retention involving tetramethylene-*1,2*-d_2. Tetramethylene-d_4 experiences no mass-based preference because the biradical termini are identical.[62]

Goldstein[3] reports $R_a = 120$, $F_{cyc} = 0.4$ for tetramethylene-d_4. Substitution into eq 6 yields a net retention in cyclization products equal to 1/97 which is then used in eq 4 with $n = 2$ and $(k_{rot}/k_{cyc})_{calc} = 2.9$ to deduce $2p - 1 = 0.19$, the net retention for a single stereorandom step that is presumably independent of isotopic substitution (e.g., a dynamical preference for 0 twist). To apply this to tetramethylene-*1,2*-d_2 derived from the diazene we add the kinematic preference for CH_2 rotation to get $2p - 1 = 0.19 + 0.10 = 0.29$. Inserting this into eq 4 with Dervan's reported value[2a] of $F_{cyc} = 0.31$ and with $n = 1$ predicts a net retention of 1/9.9 in the cyclization products which is then substituted into eq 6 to obtain $R_a = 14$, within experimental error of the reported value of 12 ± 3.[2a] Therefore *one adjustable parameter accommodates both R_a values*. The assumption about CH_2 vs CHD rotation involves no adjustable parameters. If it is not made, the value of $2p - 1 = 0.19$ predicts $R_a = 23$ in Dervan's experiment, qualitatively in the right direction but off by a factor of 2.

No explicit $k_{rot}:k_{cyc}:k_{frag}$ ratios have been reported in products derived from cyclobutane-d_2. However, Chickos[5a] reported that optical vs geometric isomerization of *trans*-cyclobutane-*1,2*-d_2 was consistent with a rotationally random biradical, as expected for two stereorandom steps in Scheme V. Starting from *cis*-cyclobutane-*1,2*-d_2, Lewis and Baldwin[4] reported a larger amount of net retention in ethenes at 980–1130 K than Goldstein[3] or Dervan[2a] reported at ca. 700 K. The expected increase in concerted fragmentation (via both **GF** and **GT**) at high temperature may contribute to the amount of retention.

The ability of Scheme V to accommodate Goldstein's[3] and Dervan's[2a] results is encouraging, but more work is necessary to judge the validity of the shared transition state model. Uncertainies in net retention are ca. 20–50%, which make it hard to decide how far p and q differ from 1. A potential problem is that p and q need not be the same. The results[2a,3] can be fit with $p = q$, but experimental uncertainties allow p and q to be different.

Carpenter[63] has advocated a dynamically determined model of thermal isomerizations for reactions with much larger stereochemical preferences than tetramethylene. In discussing these reactions he has emphasized the determinism of the classical equations of nuclear motion. We have emphasized the unpredictability associated with shared transition states on a flat PES. The two positions are not contradictory but are different aspects of the same phenomenon. Carpenter[64] proposed a method for predicting product ratios that shows promise in the reactions he has analyzed but may not be suitable for tetramethylene. In this method the probability of forming a product is proportional to the dot product of the transition vector with a vector pointing toward the local minimum of the product. The rationale is that most reactive trajectories are pointed along the transition vector as they emerge from the transition state. This is likely to work when the transition state is a narrow bottleneck, because reactive trajectories have nowhere else to go. Tetramethylene, however, has no steep walls on the sides of saddle points to enforce directionality on trajectories passing over those saddle points. With two or more processes sharing the same transition state, it is likely that trajectories approach and emerge from each transition state over a wide range of directions, rather than closely following the transition vector.

Recent computations of the stereochemistry of trimethylene,[65,66] which does not reside in a free energy minimum at typical temperatures,[37b] show that it shares tetramethylene's propensity for stereorandom reactions. Accurate calculations suggest that the transition state energies for single and double epimerization of cyclopropane are very close.[65] In fact, disrotatory double epimerization and single epimerization share the same transition structure of C_s symmetry,[65a] which is 1.5 kcal/mol higher by ZPE-corrected 2-in-2 SDCI/6-31G* than the transition state for conrotatory double epimerization in C_2 symmetry.[67] In our own examination of trimethylene, we verified these results and also found that the reported[65] transition state for single epimerization in C_1 symmetry, 0.56 kcal/mol higher than the C_s transition state with ZPE-corrected SDCI/6-31G*,[67] mediates both conrotatory and disrotatory double epimerization via two separate non-IRC paths in addition to single epimerization via the IRC path.[68] Trimethylene therefore joins tetramethylene as a molecule in which transition states mediate multiple reactions.

In many mechanisms it happens that two products share the same rate limiting step and diverge from a common intermediate in the product forming step. The same formal sequence occurs in the ring opening of cyclobutane except that the rate limiting transition state C* leads *immediately* to the post transition state product-forming step which produces stereoisomeric biradical "products". The formal similarity suggests that a more sophisticated theory may be able to establish criteria for locating bottlenecks in phase space leading to different products in the post transition state product determining region. This requires an insight into intramolecular vibrational energy flow.[69] This difficult problem in nonlinear dynamics may turn out to be directly relevant to the product distributions of biradicals.

(61) Berne, B. J. In *Physical Chemistry, An Advanced Treatise*; Henderson, D., Ed.; Academic Press: New York, Vol. VIIIB, p 683.

(62) This unusual rotational isotope effect has been discussed without reference to partition functions because all processes share the same C* transition state. In a possible experimental test, tetramethylene-*1,1,2,2,3,4*-d_6 would favor inversion instead of retention because CHD should rotate faster than CD_2. Competing dynamical preferences not based on mass would presumably also exist.

(63) (a) Carpenter, B. *Acc. Chem. Res.* **1992**, *25*, 520. (b) Carpenter, B. *J. Am. Chem. Soc.* **1985**, *107*, 5730. (c) Newman-Evans, R.; Simon, R.; Carpenter, B. *J. Org. Chem.* **1990**, *55*, 695.

(64) (a) Peterson, T.; Carpenter, B. *J. Am. Chem. Soc.* **1992**, *114*, 766. (b) Lyons, B.; Pfeifer, J.; Peterson, T.; Carpenter, B. *J. Am. Chem. Soc.* **1993**, *115*, 2427.

(65) (a) Getty, S.; Davidson, E. R.; Borden, W. T. *J. Am. Chem. Soc.* **1992**, *114*, 2085. (b) Yamaguchi, Y.; Schaefer, H. F., III *Chem. Phys. Lett.* **1991**, *185*, 143.

(66) Reference 65b contains an error originally reported in: Yamaguchi, Y.; Osamura, Y.; Schaefer, H. F., III *J. Am. Chem. Soc.* **1983**, *105*, 7506. Edge-to-face trimethylene (EF), with C_s symmetry, is reported to have one negative eigenvalue of the second derivative matrix, with a TCSCF wave function (same as 2-in-2 CAS) and 3 basis sets, one of which was the DZ basis set of ref 24. Using 2-in-2/DZ we found that EF actually has two negative eigenvalues, and obtained virtually identical results for 2-in-2/6-31G. We verified the authors' TCSCF/DZ energy and geometry for EF, but their frequencies are incorrect. For the C_{2v} edge-to-edge structure we reproduced their TCSCF/DZ energy, geometry, and frequencies exactly.

(67) We independently calculated the structures and energies reported in Table II of ref 65a, which did not report ZPEs.

(68) C. Doubleday, unpublished results; presented in preliminary form at the meeting in ref 1b.

(69) Hase, W. L., Ed. *Advances in Classical Trajectory Methods*; JAI Press: Greenwich, CT, 1992; Vol. 1.

Summary and Conclusions. (1) *gauche*- and *trans*-tetramethylene are entropy-locked biradicals at experimental temperatures. Reasonable values of the temperature-dependent free energy barriers for cyclization, fragmentation, and gauche-trans interconversion are calculated by CVT. In this calculation it is important to model the internal rotations reasonably. Harmonic partition functions underestimate the change in ΔG along the path. (2) *trans*-Tetramethylene serves as a means of interconverting *cis*- and *trans*-ethene-d_2 but does not lead to any significant amount of cyclization. The gauche conformer appears to be the common biradical intermediate invoked by experimentalists. (3) The path of lowest potential energy for cyclization of *gauche*-tetramethylene involves a CH_2 twist. Woodward–Hoffmann preferences still exist even in a 1,4-biradical. (4) At $\geq$700 K, nonconcerted and concerted mechanisms share the same transition state **C**‡ for cyclization and ring opening. The calculation does not predict the partitioning between the two mechanisms, but it is consistent with predominant nonconcerted reaction. (5) Theory and experiment are consistent with a generalized common biradical in which k_{frag}/k_{cyc} is independent of precursor but whose stereochemical dynamics depend on the precursor. This property emerges from a shared transition state model in which cisoid and transoid biradicals cyclize via the same transition state **C**‡ and fragment via the same transition state **GF**.‡ In terms of this model a new parameter, the stereochemical partitioning fraction, must be introduced into the kinetic scheme. Partitioning fractions are dynamically determined and are not predictable by transition state theories.

Acknowledgment. We gratefully acknowledge support by the National Science Foundation, Grants CHE-8722164 and CHE-9024571. We also acknowledge generous allocations of computer resources on the Cray Y-MP/48 and Y-MP/832 at the Pittsburgh Supercomputing Center. The author thanks Professors James McIver, Michael Page, and Bruce Berne for valuable discussions.

Supplementary Material Available: Tables of internal coordinates for ten stationary points, frequencies, and free energies and figures showing energy and geometry changes along non-IRC paths plus (24 pages). Ordering information is given on any current masthead page. This material is contained in many libraries on microfiche, immediately follows this article in the microfilm version of the journal, and can be ordered from the ACS; see any current masthead page for ordering information.